

1 **A δ -cell subpopulation with a pro- β -cell identity contributes to efficient age-independent**
2 **recovery in a zebrafish model of diabetes**

3
4 Claudio A. Carril Pardo^{1¶}, Laura Massoz^{1¶}, Marie A. Dupont^{1¶}, David Bergemann¹, Jordane
5 Bourdouxhe¹, Arnaud Lavergne^{1,2}, Estefania Tarifeño-Saldivia^{1,3}, Christian S. M. Helker⁴,
6 Didier Y. R. Stainier⁴, Bernard Peers¹, Marianne L. Voz¹ and Isabelle Manfroid^{1*}

7
8
9 **Author Affiliations**

10 ¹Zebrafish Development and Disease Models laboratory, GIGA-Stem Cells, University of
11 Liège, Liège, Belgium

12 ²GIGA-Genomics core facility, GIGA, University of Liège, Liège, Belgium

13 ³Gene Expression and Regulation Laboratory, Department of Biochemistry and Molecular
14 Biology, University of Concepción, Concepción, Chile

15 ⁴Department of Developmental Genetics, Max Planck Institute for Heart and Lung Research,
16 Bad Nauheim, Germany

17 ¶ Authors contributed equally (Claudio A. Carril Pardo, Laura Massoz and Marie A. Dupont)

18

19 *Corresponding author:

20 Email address: isabelle.manfroid@uliege.be

21 **Abstract**

22 Restoring damaged β -cells in diabetic patients by harnessing the plasticity of other pancreatic
23 cells raises the questions of the efficiency of the process and of the functionality of the new
24 *Insulin*-expressing cells. To overcome the weak regenerative capacity of mammals, we used
25 regeneration-prone zebrafish to study β -cells arising following destruction. We show that
26 most new *insulin* cells differ from the original β -cells as they coexpress Somatostatin and
27 Insulin. These bihormonal cells are abundant, functional and able to normalize glycemia.
28 Their formation in response to β -cell destruction is fast, efficient and age-independent.
29 Bihormonal cells are transcriptionally close to a subset of δ -cells that we identified in control
30 islets and which are characterized by the expression of *somatostatin 1.1* (*sst1.1*) and by genes
31 essential for glucose-induced Insulin secretion in β -cells such as *pdx1*, *slc2a2* and *gck*. We
32 observed *in vivo* the conversion of monohormonal *sst1.1*-expressing cells to *sst1.1+* *ins+*
33 bihormonal cells following β -cell destruction. Our findings support the conclusion that *sst1.1*
34 δ -cells possess a pro- β identity enabling them to contribute to the neogenesis of Insulin-
35 producing cells during regeneration. This work unveils that abundant and functional
36 bihormonal cells benefit to diabetes recovery in zebrafish.

37 **Introduction**

38 Insulin-producing β -cells reside in pancreatic islets where they are intermingled with other
39 endocrine cells such as α -cells, secreting glucagon (Gcg), and δ -cells secreting somatostatin
40 (Sst). Elevation of extracellular glucose concentration triggers glucose uptake by β -cells
41 through the glucose transporter GLUT2 (*slc2a2*). Glucose is then metabolized to generate
42 ATP which will trigger the closure of the K_{ATP} channel formed by Kir6.2 (*kcnj11*) and SUR1
43 (*abcc8*), membrane depolarization, Ca^{2+} influx and release through exocytosis of insulin
44 secretory granules into the blood. In mature β -cells, this process is further amplified by other
45 molecules such as amino acids, fatty acids, hormones (incretins GLP-1, GIP) and neural
46 factors (dopamine, adrenaline...) via the cAMP messenger. Dysfunction of these processes
47 leads to impaired insulin secretion, chronic hyperglycemia and diabetes. In Type 2 diabetes,
48 chronic glucolipotoxic stress ultimately provokes β -cell failure and death. In Type 1 diabetes,
49 on the other hand, the destruction of β -cells is mediated by an autoimmune attack.

50 Human adult β -cells are quiescent and barely possess the capacity to compensate their
51 destruction through increased proliferation. Alternative mechanisms inferred from studies in
52 mice revealed the striking plasticity of other pancreatic endocrine cell types towards the β -cell
53 phenotype. For example, Ins⁺ Gcg⁺ bihormonal cells form after acute β -cell destruction
54 mediated by transgenic expression of the diphtheria toxin receptor (DTR) in adult mice (Thorel
55 et al., 2010). These cells derive from a small fraction of α -cells that switch on the β -cell
56 markers Pdx1, Nkx6.1 and Ins through direct conversion, leading to restoration of about 10%
57 of the β -cell mass after 10 months. As this process is quite slow and inefficient, adult DTR
58 mice do not survive without injection of insulin during the first months after ablation. In
59 contrast, at juvenile stages, β -cell neogenesis occurs from transdifferentiation of δ -cells
60 (Chera et al., 2014). In this case, δ -cells dedifferentiate, lose *Sst* expression, replicate and

61 redifferentiate into β -cells. About 23% of the initial β -cell mass has recovered 4 months after
62 ablation emphasising faster and more efficient improvement of glycemia than in adult mice.
63 Very recently, a rare population of pancreatic polypeptide (Ppy)-expressing γ -cells has also
64 been shown to display plasticity and to activate *Ins* expression in response to β -cell injury
65 (Perez-Frances et al., 2021). Hence, various pancreatic islet cells possess a remarkable
66 plasticity yet the regeneration potential is generally limited in adult mammals.

67 In contrast to the limited regeneration capacity of adult mammals, zebrafish are notorious for
68 their potent, spontaneous and rapid regeneration of β -cells from larval to adult stages (Curado
69 et al., 2007; Delaspre et al., 2015; Ghaye et al., 2015; Moss et al., 2009; Ninov et al., 2013;
70 Pisharath & Parsons, 2009; Ye, Robertson, Hesselton, Stainier, & Anderson, 2015). In
71 zebrafish, α -cells transdifferentiate into *Ins*-expressing cells after β -cell destruction (Ye et al.,
72 2015). On the other hand, unlike mouse models in which regeneration via progenitors or
73 precursors is debated, β -cell neogenesis is well recognised in zebrafish to involve regenerative
74 processes from progenitor-like cells present in the ducts (Delaspre et al., 2015; Ghaye et al.,
75 2015; Ninov et al., 2013). β -cell destruction is accomplished in zebrafish using a chemo-
76 genetic system based on the transgenic expression of the bacterial nitroreductase (NTR) under
77 the control of the *ins* promoter where cell death is induced by a nitroaromatic prodrug
78 (Bergemann et al., 2018; Curado et al., 2007; Pisharath & Parsons, 2009). In adults, after a
79 huge rise of glycemia within 3 days, the pancreas is replenished with new β -cells in 2 to 3
80 weeks which correlates to a return to normoglycemia.

81 *De novo* formation of β -cells in order to repair damaged islets constitutes a promising
82 therapeutic perspective for diabetic patients. However, new β -cells could show differences in
83 their number and identity impacting on their activity. For example, the presence in mice of
84 Gcg^+ Ins^+ cells, though apparently functional, should be considered cautiously as

85 inappropriate differentiation of β -cells and impaired maturation or identity are common
86 shortcoming in diabetes ((Moin & Butler, 2019) for review).

87 Using the larval and adult zebrafish as regeneration models, we investigated the identity of
88 regenerated β -cells and discovered that most new *ins*-expressing cells are *Ins*⁺ *Sst1.1*⁺
89 bihormonal cells. We identified a specific δ -cell subpopulation distinct from the previously
90 identified zebrafish *sst2* δ -cells that is characterized by the expression of *sst1.1* and of several
91 important β -cell features. The transcriptomic profile of bihormonal cells is also very close to
92 the *sst1.1* δ -cells, making them resemble β/δ hybrids. By *in vivo* imaging of larvae, we
93 observed the appearance of *ins*-expressing bihormonal cells from monohormonal *sst1.1* δ -
94 cells early after β -cell ablation. We also provide evidence that pancreatic ducts contribute to
95 the pool of bihormonal cells. Furthermore, bihormonal cells are abundant in the regenerated
96 pancreas and able to normalize glycemia after a glucose challenge. Our findings show the
97 importance of bihormonal cells in the spontaneous recovery of diabetic zebrafish.

98

99 **Results**

100 *Most regenerated β -cells coexpress Ins and Sst in adult zebrafish*

101 To characterize the new β -cells after regeneration, we used 6- to 10-month old *Tg(ins:NTR-*
102 *P2A-mCherry)* (Bergemann et al., 2018) adult fish to first ablate β -cells. Basal blood glucose
103 was monitored to evaluate ablation (3 days post treatment, dpt) and regeneration (20 dpt). As
104 expected, fasting basal blood glucose dramatically raised at 3 dpt compared to CTL fish
105 which reflected efficient ablation (Figure 1A and Figure 1-Source Data 1). After 20 days,
106 glycemia was impressively improved though still slightly above control values. A preliminary
107 RNAseq experiment on mCherry⁺ cells isolated from the main islet of *Tg(ins:NTR-P2A-*

108 *mCherry*) adult fish 2 months after ablation revealed strong expression of the *sst1.1* gene in
109 regenerated β -cells just below *ins* (Figure 1-figure supplement 1), thereby suggesting that
110 regenerated β -cells are bihormonal. As blood glucose is nearly normalized after 20 days, we
111 characterized these cells at this time point. Immunofluorescence on regenerated 20 dpt islets
112 showed many *Ins*⁺ cells that also displayed *Sst* immunolabelling (Figure 1B). In contrast,
113 control islets showed robust staining of the endogenous *Ins* and *Sst* hormones without
114 appreciable overlap, thus demarcating monohormonal β - and δ -cells (Figure 1B). We next
115 created a *Tg(sst1.1:eGFP)* reporter line driving GFP in *sst1.1*-expressing cells. This transgene
116 was not active in β -cells of control islets (Figure 1-figure supplement 2). Similar to what was
117 observed with the endogenous *Sst* and *Ins* proteins, regenerated 20 dpt islets of
118 *Tg(sst1.1:eGFP); Tg(ins:NTR-P2A-mCherry)* fish contained many cells coexpressing GFP
119 with *mCherry*, while GFP and *mCherry* labelled distinct cells in control islets (Figure 1C).
120 Strikingly, double positive cells could already be detected 3 days after ablation though they
121 displayed low levels of *mCherry*.

122 We next quantified *ins*⁺ β -cells, *sst1.1*⁺ cells and double *ins*⁺ *sst1.1*⁺ cells by measuring the
123 number of *mCherry*⁺, GFP⁺, and GFP⁺ *mCherry*⁺ cells, respectively, in *Tg(sst1.1:eGFP);*
124 *Tg(ins:NTR-P2A-mCherry)* adult fish. The main islet was obtained by dissection and the
125 different cell populations were analysed by FACS (Figure 1D-G, Figure 1-figure supplement
126 3 and Figure 1-Source Data 2). At 3 and 20 dpt, we observed a drastic loss of *mCherry*⁺
127 (GFP⁻) β -cells with a drop to 3.2% of the initial β -cell mass at 3 dpt (Figure 1E). In contrast, a
128 large population of double GFP⁺ *mCherry*⁺ cells appeared that represented 43% of the initial
129 β -cell mass (Figure 1F). These cells still persisted at 20 dpt and they made up at this stage
130 98% of the *ins*-expressing cells. At 20 dpt, *mCherry*⁺ GFP⁻ β -cells still constituted a very
131 minor population. (Figure 1E). After ablation, the amount of GFP⁺ *mCherry*⁻ cells also
132 decreased (Figure 1G).

133 In conclusion, these results indicate that *ins*⁺ *sst1.1*⁺ bihormonal cells rapidly appear in the
134 main islet after β -cell ablation in adult fish and persist steadily for at least 20 days. They
135 constitute the vast majority of the new *ins*-expressing cells following ablation.

136

137 *Genesis of bihormonal cells also occurs during regeneration in larval stages and is*
138 *independent of the ablation model*

139 As in mouse the process of bihormonal cells (in that case Gcg⁺ Ins⁺) formation after β -cell
140 ablation is specific to adult stages (Thorel et al., 2010)(Chera et al., 2014), we next asked
141 whether Sst1.1⁺ Ins⁺ bihormonal cells also appear in zebrafish larvae. We therefore
142 performed the ablation in *Tg(sst1.1:eGFP); Tg(ins:NTR-P2A-mCherry)* at 3 days post
143 fertilization (dpf) and assessed the expression of *ins*:mCherry and *sst1.1*:GFP. Like in adults,
144 bihormonal cells were detected 3 days after ablation (3 dpt, 6 dpf) (Figure 2A-B). We
145 confirmed by *in situ* hybridization detecting the endogenous mRNAs that these bihormonal
146 cells express *sst1.1* together with *ins* (Figure 2C). This experiment also revealed that they do
147 not coexpress *sst2* (Figure 2C).

148 Then we questioned if the bihormonal cells can also be induced using another system of β -cell
149 destruction. We chose the Diphtheria Toxin chain alpha (DTA) suicide transgene which has
150 previously been used to efficiently ablate β -cells (Ninov et al., 2013). Ablation was achieved
151 in *Tg(ins:lox-mCherry-lox-DTA); Tg(ins:CRE-ERT2)* larvae by performing a 4-OHT
152 treatment at 7 dpf and the larvae were then analysed at 16 dpf (Figure 2-figure supplement 1).
153 Similar to our observations with the NTR system, Ins and Sst immunofluorescence revealed
154 many coexpressing cells.

155 In conclusion, these data demonstrate that there is no specific competent stage for the
156 formation of *Ins⁺ Sst1.1⁺* bihormonal cells in zebrafish. In addition, this process does not
157 depend on the method of ablation.

158

159 *Most bihormonal cells do not derive from pre-existing β -cells*

160 To explore the possibility that bihormonal cells derive from pre-existing β -cells spared by the
161 ablation, β -cells were traced before ablation using *Tg(ins:CRE-ERT2); Tg(ubb:loxP-CFP-*
162 *loxP-zsYellow); Tg(sst1.1:GFP); Tg(ins:NTR-P2A-mCherry)* fish. As bihormonal cells were
163 also observed at 6 dpf, we used larvae to tackle their origin by CRE-mediated recombination
164 (Hans, Kaslin, Freudenreich, & Brand, 2009; Mosimann et al., 2011). We treated the larvae
165 with 4-OHT at 6 dpf to label the β -cells and performed the ablation the next day (Figure 2D).
166 We found that, 7 days after ablation, only 10% of the bihormonal cells were positive for the
167 *zsYellow* lineage tracer (Figure 2E-E' and 2H). To ensure that this low level was not due to
168 an inefficient tracing, we checked non-ablated larvae and found that 94% of the β -cells were
169 labelled with *zsYellow* (Figure 2F-G). In addition, the *sst1.1:GFP⁺* cells were not labelled
170 (Figure 2F). These data demonstrate good efficiency and specificity of the tracing. Based on
171 these observations, we can conclude that some bihormonal cells originate from pre-existing β -
172 cells but the majority arises from non- β origin(s).

173

174 *ins⁺ sst1.1⁺ bihormonal cells share similarities with β - and δ -cells, and possess the basic*
175 *machinery for glucose responsiveness*

176 In order to characterize the *ins⁺ sst1.1⁺* bihormonal cells after regeneration, we analysed
177 their transcriptomic profile. To this end, double *GFP⁺ mCherry⁺* cells were isolated by FACS

178 from the main islet of *Tg(sst1.1:eGFP); Tg(ins:NTR-P2A-mCherry)* adult fish at 20 dpt.
179 Control β -cells (mCherry+ GFP-) were obtained from age-matched, non-ablated, transgenic
180 fish. We compared their RNAseq profiles and identified 887 DE genes with a higher
181 expression in bihormonal cells and 705 DE genes higher in β -cells (Padj<0.05 and above 2-
182 fold differential expression) (Figure 3A-B and Figure 3-Source Data 1). In accordance with
183 the weak mCherry fluorescence harboured by GFP+ mCherry+ cells as compared to native β -
184 cells, the expression of *ins* in bihormonal cells was 5-fold below its typical level in β -cells
185 (Figure 3C). Also, as expected, the δ -cell hormone *sst1.1* was sharply overexpressed in
186 bihormonal cells (209-fold) compared to its basal level in β -cells, and was even the top
187 hormone just above *ins* (Figure 3C). The other pancreatic hormones known in zebrafish,
188 *sst1.2*, *sst2*, *gcga*, *gcgb* and *ghrl*, were detected at much weaker levels in both *ins*+
189 populations (Figure 3C). Accordingly, Gcg protein was undetectable in bihormonal cells by
190 immunofluorescence (Figure 3-figure supplement 1). Collectively, these data confirm that
191 bihormonal cells coexpress high levels of two main hormones, *ins* and *sst1.1*, at both the
192 mRNA and protein levels.

193 To further characterize these bihormonal cells, we assessed the expression of transcription
194 factors important for β -cell development and identity in zebrafish and mouse/human (see list
195 in Figure 3-figure supplement 2). We first checked the expression of the pan-endocrine genes
196 *neurod1*, *pax6b* and *isl1* and found similar expression (Figure 3C). We also examined the
197 expression of *pdx1*, a transcription factor essential for *ins* expression in β -cells. *pdx1* was
198 equally expressed in both native β -cells and post-regeneration GFP+ mCherry+ cells. We next
199 evaluated the β -cell identity of bihormonal cells by interrogating the expression of zebrafish
200 β -cell markers. We defined these markers as genes enriched in β -cells (>4-fold) versus the
201 other main pancreatic cell types (α -, *sst2* δ -cells, acinar and ductal cells) based on previous

202 RNAseq data (Tarifeño-Saldivia et al., 2017) (Figure 3-Source Data 2). This list of β -cell
203 genes includes *nkx6.2*, a previously identified β -cell marker in zebrafish (A.-C. Binot et al.,
204 2010)(Tarifeño-Saldivia et al., 2017) which is the equivalent of *Nkx6.1* in mouse/human β -
205 cells (Figure 3-figure supplement 2). More than half of the 62 “ β -cell genes” were expressed
206 at similar levels in both *bona fide* β -cells and post-regeneration bihormonal cells. In contrast,
207 27 β -cell genes showed either over- or underexpression (Figure 3D). In particular, 18 β -cell
208 genes were underexpressed in bihormonal cells like, for example, *nkx6.2* which was not
209 expressed at all (Figure 3E). We also looked at markers of dedifferentiation and found that the
210 zebrafish pancreatic progenitor markers *nkx6.1*, *sox9b* and *ascl1b*, were barely expressed in
211 bihormonal cells, like in control β -cells.

212 When considering key genes for β -cell function and maturation, *i.e.* glucose sensing, uptake,
213 Ins maturation and secretion, many were expressed at comparable levels in both cell types,
214 such as notably *slc2a2*, *pcsk1*, *abcc8* and *snap25a* (Figure 3E). *ucn3l*, a marker of mature β -
215 cells in mammals (Blum et al., 2012) and zebrafish (Singh et al., 2017), was overexpressed in
216 bihormonal cells.

217 Gene Ontology (GO) analysis of the genes overexpressed in bihormonal cells compared to β -
218 cells showed that the top significant biological processes were related to adhesion and
219 neuronal synapses with many genes that are known in β -cells to be important for Insulin
220 processing and exocytosis (Figure 3F-G and Figure 3-Source Data 3). Other processes
221 included intracellular Calcium and cAMP signalling (Figure 3F-G and Figure 3-Source Data
222 3). These data strongly suggest that bihormonal cells, like β -cells, are excitable cells with the
223 capacity to secrete Insulin in response to glucose.

224 Altogether, these data indicate that bihormonal cells possess the molecular bases of functional
225 mature β -cells such as a glucose-responsiveness and hormone secretion machinery. However,

226 although many β -cell genes are similarly expressed between bihormonal and β -cells,
227 bihormonal cells display a divergent identity such as lack of the zebrafish β -cell marker
228 *nkx6.2* and strong expression of *sst1.1*.

229

230 *Bihormonal cells constitute the main source of Insulin in regenerated zebrafish and restore*
231 *blood glucose homeostasis*

232 The basal glycemia of regenerated fish is nearly normalized after 20 days, strongly suggesting
233 that bihormonal cells - that represent 98% of the Ins-producing cells - contribute to blood
234 glucose control. To exclude the possibility that glycemia is regulated by a population of
235 genuine monohormonal β -cells regenerated outside the main islet, we analysed the pancreatic
236 tail. Indeed, zebrafish possess smaller secondary islets scattered in the pancreatic tail in
237 addition to the large main islet located in the head. Similar to the main islets, regenerated 20
238 dpt secondary islets harboured many bihormonal cells and very scarce monohormonal β -cells
239 (Figure 4A-B and Figure 4-Source Data 1). Thus, bihormonal cells constitute the predominant
240 source of Ins throughout the whole pancreas.

241 To assess the functionality of adult bihormonal cells, we performed a glucose tolerance test
242 and blood glucose levels were followed after an intraperitoneal injection of D-Glucose.
243 Regenerated fish 20 days after β -cell ablation displayed completely normal glucose tolerance
244 (Figure 4C and Figure 4-Source Data 2). Together, all these data support the conclusion that
245 the bihormonal cells are responsible for the normalization of glycemia and glucose tolerance
246 in regenerated zebrafish.

247

248 *sst1.1 δ -cells are distinct from sst2 δ -cells and display similarities with β -cells*

249 Given the expression of *sst1.1* in bihormonal cells, we sought to characterize the *sst1.1*-
250 expressing cells in normal islets without ablation. Previous transcriptomic studies of
251 pancreatic cells detected three *Sst* genes in normal adult pancreatic islets, *sst1.1*, *sst1.2* and
252 *sst2* (Spanjaard et al., 2018; Tarifeño-Saldivia et al., 2017). However, so far, only the *sst2* δ -
253 cells, which also express *sst1.2*, have been fully characterized (Tarifeño-Saldivia et al., 2017).
254 We thus isolated the *sst1.1*-expressing GFP⁺ cells from control non-ablated islets of
255 *Tg(sst1.1:eGFP); Tg(ins:NTR-P2A-mCherry)* adult fish to determine their transcriptome.
256 Close examination of these *sst1.1*:GFP⁺ cells by flow cytometry actually distinguished two
257 subpopulations recognised by different levels of GFP fluorescence, GFP^{low} and GFP^{high}
258 (Figure 5-figure supplement 1A). The GFP^{high} population represented 35% of all GFP cells.
259 The presence of cells with high and low GFP were also observed by *in situ* by
260 immunofluorescence on fixed whole pancreas (Figure 5A).

261 The transcriptomic profile of the two GFP populations was obtained (Figure 5-figure
262 supplement 1B). Principal Component Analysis (PCA) unveiled that GFP^{high} cells are very
263 similar to bihormonal cells (Figure 5B). In addition, they are also more similar to β -cells than
264 GFP^{low} cells. Clustering analysis of the two GFP populations, the bihormonal cells and the
265 other endocrine cells (α , β and *sst2* δ -cells (Tarifeño-Saldivia et al., 2017)) also showed that
266 the GFP^{high} cells cluster together with bihormonal cells and apart from the GFP^{low} cells
267 (Figure 5C). Indeed, GFP^{low} cells were closer to *sst2* δ -cells than to the other endocrine
268 subtypes. Comparison of the two GFP populations identified 975 and 1206 DE genes
269 overexpressed in GFP^{high} and GFP^{low}, respectively (FC>2, Padj<0.05) (Figure 5D and Figure
270 5-Source Data 1). *sst1.1* was by far the predominant *Sst* gene expressed in GFP^{high} cells
271 (Figure 5E). On the opposite, *sst2* was predominant in GFP^{low} cells though these cells also
272 expressed *sst1.2* and *sst1.1* at lower levels. In addition, while both populations expressed the
273 universal δ -cell marker *hhex*, other previously identified markers of zebrafish *sst2* δ -cells such

274 as *cdx4*, *tbx2b* and *map3k15* (Tarifeño-Saldivia et al., 2017) were specific to GFP^{low} cells
275 (Figure 5F-G). Indeed, more than 75% of the *sst2* δ -cell genes (enriched >4-fold based on
276 previous data (Tarifeño-Saldivia et al., 2017)) were also enriched in GFP^{low} cells (Figure 5F
277 and Figure 5-Source Data 2). Ectopic activity of the *sst1.1:GFP* transgene in the *sst2* δ -cells
278 was confirmed by ISH showing *sst2* probe signal exclusively in the weakest GFP⁺ cells
279 (Figure 5-figure supplement 1C). These data show that the GFP^{low} population contains *sst2* δ -
280 cells, while the GFP^{high} population consists of a pure and distinct δ -cell population
281 characterized by strong *sst1.1* expression. These δ -cells will be named *sst1.1* δ -cells hereafter.

282 Focusing on the *sst1.1* δ -cells, we noticed high expression of *pdx1* (Figure 5G). In addition to
283 being expressed in all β -cells, *Pdx1* in mammals is also expressed in a subset of δ -cells (Piran
284 et al., 2014; Segerstolpe et al., 2016). In zebrafish, *pdx1* is expressed in β -cells but not in *sst2*
285 δ -cells (Tarifeño-Saldivia et al., 2017). In agreement with the transcriptome of *sst1.1* δ -cells,
286 Pdx1 immunolabelling was confirmed in a subset of Sst⁺ cells on paraffin section through the
287 adult main islet (Figure 5H). Next, we investigated the expression of the 62 zebrafish “ β -cell
288 genes”. Strikingly, most of them (36/62), such as *ucn3l*, were found enriched in *sst1.1* δ -cells
289 (Figure 5F-G and Figure 5-Source Data 2) while none was preferentially expressed in the
290 GFP^{low} cells. By immunofluorescence, Ucn3 decorated β -cells in control islets and,
291 additionally, an even more intense staining was detected in a subset of GFP^{high} cells. After
292 ablation, the anti-Ucn3 also marked bihormonal cells, confirming our RNAseq data (Figure
293 5I). Based on these new transcriptomic datasets, we defined the genes selectively enriched
294 (>4-fold) in *sst1.1* δ -cells versus the other endocrine cell types already available (*sst2* δ , β and
295 α) and identified 152 specific *sst1.1* δ -cell markers, among which *bdnf*, *cdh10a*, *sox11b* and
296 *dkk3b* (Figure 5-Source Data 3). An updated list of 60 markers enriched in β -cells versus
297 *sst1.1* δ -cells, α and *sst2* δ -cells altogether could also be defined. Our RNAseq data also

298 revealed that *dkk3b* and *ucn3l*, previously attributed to β -cells, were even more enriched in
299 *sst1.1* δ -cells.

300 Top GO terms overrepresented in GFP^{low}/*sst2* δ -cells (Figure 5J and Figure 5-Source Data 4)
301 were related to neuron differentiation, adhesion and Wnt signalling. Top most significant GO
302 terms and pathways in *sst1.1* δ -cells (Figure 5J and Figure 5-Source Data 5) included
303 “biological adhesion” and proprotein convertases important in the secretory pathway such as
304 *pcsk1* and *pcsk2*. Together with *gck*, *g6pcb*, *slc2a2* and *hk2* associated with “metabolism of
305 carbohydrates”, these signatures suggest some competence of *sst1.1* δ -cells for glucose-
306 responsiveness and hormone secretion.

307 Overall, these data unveil that *sst1.1* δ -cells represent a distinct δ -cell population possessing
308 basic features of β -cells and sensors to integrate Ins signalling, glucose metabolism and carry
309 hormone secretory activity.

310

311 *Monohormonal sst1.1-expressing cells transcriptionally activate the ins gene following β -cell*
312 *ablation*

313 The transcriptomic profile of *sst1.1* δ -cells suggests that they represent a promising candidate
314 as cellular origin of bihormonal cells. In line with a conversion of *sst1.1* δ -cells to bihormonal
315 cells, the number of monohormonal GFP^{high} cells was reduced after ablation in adult fish
316 compared to CTL (from 979 cells to 315 at 20 dpt) (Figure 6A, Figure 6-Source Data 1). To
317 test the hypothesis of a direct conversion of *sst1.1* δ -cells, we followed the appearance of
318 bihormonal cells by *in vivo* time lapse imaging of the main islet in *Tg(sst1.1:eGFP);*
319 *Tg(ins:NTR-P2A-mCherry)* larvae after ablation from 3 to 4 dpf. Figure 6B-B’ show mCherry
320 fluorescence progressively appearing in monohormonal *sst1.1*:GFP⁺ cells presenting strong

321 GFP fluorescence, most likely *sst1.1* δ -cells. These results indicate the activation of the *ins*
322 promoter of the *ins:mCherry* transgene in *sst1.1:eGFP* cells and suggest that at least some
323 *sst1.1* δ -cells directly convert into bihormonal cells immediately after ablation.

324

325 *Bihormonal cells have a transcriptomic profile very similar to sst1.1 δ -cells but with distinct*
326 *cell cycle signatures*

327 As the PCA and clustering analyses shown Figure 5B-C revealed that bihormonal and
328 monohormonal GFP^{high}/*sst1.1* δ -cells are transcriptionally similar, we next directly performed
329 a pairwise comparison of their transcriptome. This analysis revealed a few DE genes, with
330 293 over- and 180 underexpressed genes in bihormonal cells versus *sst1.1* δ -cells (FC 2-fold,
331 Padj <0.05) (Figure 6C and Figure 6-Source Data 2), indicating that the identity of
332 bihormonal cells is very close to *sst1.1* δ -cells. The *ins* gene was the top overexpressed gene
333 in bihormonal cells (54-fold) (Figure 6D). Among the 293 overexpressed genes in bihormonal
334 cells, 9 were β -cell markers such as *ins* and *fst11a* and, among the 180 underexpressed genes,
335 8 were *sst1.1* δ -cell markers. Both *sst1.1* and *hhex* were equally expressed, further
336 underscoring that bihormonal cells and *sst1.1* δ -cells have a close identity.

337 GO analyses of the genes overexpressed in bihormonal cells identified “ribosome”,
338 “proteasome”, “p53 signaling pathway” and “cell cycle” pathways as top enriched pathways
339 (Figure 6E and Figure 6-Source Data 3-4). To corroborate the cell cycle signature, we
340 examined Proliferating Cell Nuclear Antigen (PCNA) in the main islet of *Tg(ins:NTR-P2A-*
341 *mCherry)* adult fish. In CTL islets, PCNA immunodetection was almost absent. In contrast, it
342 was widely observed in mCherry⁺ cells at 20 dpt (Figure 6F). As mCherry⁺ cells are also
343 bihormonal, it can be concluded that PCNA is expressed in bihormonal cells. We also
344 examined Pdx1 as a proxy for β , *sst1.1*- δ and bihormonal cells (Figure 6-figure supplement

345 1A). The proportion of PCNA⁺ Pdx1⁺ cell was strongly increased in 3 and 20 dpt islets
346 compared to CTL. To assess more specifically DNA replication, we performed a 2-day
347 incorporation of the established marker of DNA synthesis EdU in *Tg(sst1.1:eGFP);*
348 *Tg(ins:NTR-P2A-mCherry)* larvae (Figure 6-figure supplement 1B). Larval *sst1.1:GFP*⁺ cells
349 and *ins:mCherry*⁺ β -cells displayed basal DNA replication (CTL). In NFP-treated larvae, the
350 few monohormonal β -cells detected 3 days post-ablation rarely incorporated EdU showing
351 that most escaping β -cells do not proliferate after ablation. In contrast, monohormonal GFP⁺
352 EdU⁺ cells were observed in similar proportion between control and ablated larvae.
353 Importantly, a significant fraction of bihormonal cells induced by the ablation showed DNA
354 replication (Figure 6-figure supplement 1B).

355 To assess p53 activity, important for cell cycle checkpoints, we also used larvae to analyse the
356 expression of p53 target genes by *in situ* hybridization. *mdm2* and *ccng1* were found induced
357 in a subset of *sst1.1:GFP*⁺ cells at 3 dpt (Figure 6G), confirming the activation of the p53
358 pathway in response to the destruction of β -cells.

359 Given the activation of the p53 pathway following β -cell ablation, and as p53 is generally
360 activated in response to cellular stress, we investigated the role of common stresses caused by
361 β -cell death like hyperglycemia, oxidative stress and impaired Insulin signalling, in
362 bihormonal cell formation. In particular, we asked whether these signals could induce by
363 themselves the formation of bihormonal cells. However, none of these stresses was sufficient
364 to trigger the formation of bihormonal cells (Figure 6-figure supplement 2).

365 Together, these results demonstrate that bihormonal cells in regenerating islets express genes
366 involved in cell cycle progression and checkpoints. In line with these findings, our data also
367 show that bihormonal cells and possibly *sst1.1* δ -cells engage in proliferation in response to
368 the ablation of β -cells.

369

370 *Bihormonal cells also arise from pancreatic ducts*

371 In zebrafish, the secondary islets originate from pancreatic duct-associated progenitors in a
372 process initiated during normal larval development (Parsons et al., 2009; Wang, Rovira,
373 Yusuff, & Parsons, 2011). Ducts also contribute to β -cell regeneration in the adult zebrafish,
374 providing new β -cells to the main and secondary islets (Delaspre et al., 2015; Ghaye et al.,
375 2015). The striking observation that the vast majority of new *ins*-expressing cells are
376 bihormonal in the entire pancreas raises the hypothesis that duct-derived Ins^+ cells also
377 express *Sst1.1*. To explore this possibility, we used larvae, a well-established model to study
378 β -cell regeneration from the ducts (Ninov et al., 2013). In this model, destruction of β -cells
379 not only induces their regeneration in the main islet but also activates duct-associated
380 progenitors to produce more β -cells. We first determined the time course of duct-derived β
381 and *sst1.1* δ -cell formation during normal development and established that they start to
382 differentiate between 7 and 10 dpf (Figure 7-figure supplement 1). Next, we used the
383 *Tg(nkx6.1:eGFP); Tg(ins:NTR-P2A-mCherry)* line, where *nkx6.1* is a marker of pancreatic
384 ducts and of duct-associated progenitors (Ghaye et al., 2015), to perform the ablation of β -
385 cells at 3 dpf, *i.e.* before the normal differentiation of β and *sst1.1* δ -cells in the tail. Thus,
386 potential Ins^+ *Sst1.1*⁺ bihormonal cells appearing in the tail after ablation are expected to
387 originate from the ducts and not from secondary β or *sst1.1* δ -cells. At 17 dpf, mCherry and
388 *Sst* immunodetection was analysed (Figure 7A-B). Double positive bihormonal cells were
389 found in the ductal *nkx6.1*:GFP⁺ domain in the tail of regenerating larvae while they were
390 almost absent in CTL ducts (Figure 7B-B'-C and Figure 7-Source Data 1). These findings
391 support that duct cells give rise to bihormonal cells during regeneration and that they
392 contribute to the overall bihormonal cell mass.

393

394 *Bihormonal cells persist long after β -cell ablation*

395 Finally, we questioned the persistence of bihormonal cells long after ablation and analysed the
396 main islet from *Tg(sst1.1:eGFP); Tg(ins:NTR-P2A-mCherry)* adult fish 4 months after
397 ablation. Surprisingly, most Ins⁺ cells still coexpressed GFP as well as high levels of Ucn3 at
398 this stage (Figure 8A), similarly to 20 dpt bihormonal cells. Bihormonal cells still constituted
399 the vast majority of *ins*-expressing cells in the main islet compared to monohormonal β -cells
400 (Figure 8B-D). This also suggests that they do not represent a transient intermediary
401 population that would ultimately resolve into *ins*-only β -cells.

402

403 **Discussion**

404 Pancreatic endocrine cell plasticity and impaired identity has emerged as an important cellular
405 adaptive behaviour in response to β -cell stress and death in human and in mammalian diabetic
406 models. Here we show that, in zebrafish, a large and predominant population of Ins⁺ Sst1.1+
407 bihormonal cells arise after β -cell destruction, confers glucose responsiveness and restores
408 blood glucose homeostasis. Moreover, contrasting with the age-dependent and limited β -cell
409 neogenesis of mouse models (Chera et al., 2014; Perez-Frances et al., 2021; Thorel et al.,
410 2010), bihormonal cell formation in zebrafish is fast and efficient and occurs all along life.

411 Our study provides an in-depth characterization of the zebrafish *sst1.1* δ -cell subpopulation.
412 The existence of two distinct δ -cell subpopulations corroborates a recent report of two clusters
413 of δ -cells detected by single cell RNAseq, one expressing *sst2/sst1.2* and the other *sst1.1*
414 (Spanjaard et al., 2018). Although our β -cell lineage tracing experiment in larvae indicates
415 that a subset of bihormonal cells derive from pre-existing β -cells, the majority have a non- β
416 origin. Here, we present evidences that bihormonal cells originate from *sst1.1* δ -cells and duct
417 cells. In contrast to *sst2* δ -cells which have previously been excluded to generate new Ins-

418 expressing cells (Ye et al., 2015), our results strongly suggest that *sst1.1* δ -cells rapidly adapt
419 to the loss of β -cells and activate *ins* expression. First, pre-existing *sst1.1* δ -cells already
420 express many genes essential for β -cells such as *pdx1*, *ucn3l* and the glucose transporter
421 *slc2a2* (Glut2). Second, *sst1.1* δ -cells and bihormonal cells have a very close transcriptomic
422 profile meaning that only minor changes in *sst1.1* δ -cells would generate bihormonal cells.
423 Third, *sst1.1* δ -cells express the basic molecular machinery for glucose-sensing, glucose- and
424 calcium-dependent stimulation of Insulin secretion and blood glucose control. Fourth, the
425 appearance of bihormonal cells during regeneration concurs with a reduction of the *sst1.1* δ -
426 cell mass. Finally, *in vivo* imaging revealed the activation of *ins* expression in *sst1.1* δ cells
427 early after ablation. All these observations support the conclusion that *sst1.1* δ -cells constitute
428 a distinct zebrafish δ -cell population expressing β -cell features enabling them to rapidly
429 reprogram to bihormonal cells by activating *ins* expression and engender functional
430 surrogate β -cells. Importantly, during the preparation of our manuscript, Singh et al. also
431 identified *sst1.1*+ *ins*+ δ/β hybrid cells in zebrafish by scRNAseq (Singh et al., 2021). They
432 also proposed the *sst1.1* δ -cells as possible cellular origin after β -cell ablation, thereby
433 consolidating our findings. A difference between our two studies, however, is that they
434 detected some hybrid *Sst1.1*+ *Ins*+ cells in control islets while we could not clearly identify
435 them, probably due to different technical approaches.

436 The fact that the bihormonal cell population is somewhat larger than the *sst1.1* δ -cell
437 population (compare 979 $\text{GFP}^{\text{high}}/\textit{sst1.1}$ δ -cells in CTL fish in Figure 6A with ~1400
438 bihormonal cells post-ablation in Figure 1F) suggests the implication of mechanisms
439 complementary to direct conversion. Indeed, beside *sst1.1* δ -cells as cellular origin of
440 bihormonal cells, our findings also point to alternative sources, i) a β -cell origin from pre-
441 existing cells spared by the ablation and ii) a ductal origin, at least in larvae. Our results show

442 that a small but significant fraction of bihormonal cells arises from β -cells. We also show that
443 bihormonal cells form in the pancreatic ducts. As ducts are present in the tail as well as in the
444 head, these results suggest a ductal contribution to the global bihormonal cell mass, *i.e.* the
445 main and secondary islets. Whether regenerating duct-derived bihormonal cells differentiate
446 via a monohormonal *sst1.1* δ -cell transitional state remains to be determined. Moreover, the
447 ducts could help repopulate the *sst1.1* δ -cells after conversion. Besides neogenesis, our results
448 suggest that proliferation contributes to the formation and/or maintenance of the pool of
449 bihormonal cells and *sst1.1* δ -cells. Notably, we observed evidences of proliferation at an
450 early stage after β -cell ablation, 3 dpt, as illustrated by replicating EdU+ bihormonal cells in
451 larvae and broad PCNA expression in adults. Interestingly, the activation of p53 indicates a
452 tight control on proliferation in bihormonal cells. At 20 dpt, the p53 pathway represents the
453 second most enriched signature in bihormonal cells, while PCNA is still widely expressed. To
454 understand this observation, it would be interesting to tackle the dynamics of cell cycle and to
455 perform a detailed analysis of different markers of cell cycle progression and checkpoints in
456 the different cell populations during regeneration.

457 The identification of bihormonal cells in zebrafish brings the question of the molecular
458 mechanisms underlying this β/δ hybrid identity. In mammals, *Pdx1* is essential for β -cell
459 function notably through activation of *Ins* and of the glucose-sensing machinery genes *Slc2a2*
460 and *Gck* (Ahlgren, Jonsson, Jonsson, Simu, & Edlund, 1998; Waeber, Thompson, Nicod, &
461 Bonny, 1996; Watada et al., 1996). *Pdx1* is also crucial to promote and maintain β -cell
462 identity as it activates β -cell genes and represses the α -cell program (Ahlgren et al., 1998; Gao
463 et al., 2014). Interestingly, *Pdx1*, also known as STF1 (Somatostatin Transcription Factor 1),
464 is expressed in a subset of mouse/human δ -cells (Piran et al., 2014; Segerstolpe et al., 2016)
465 and stimulates *Sst* expression (Leonard et al., 1993). In both murine α and γ -cells, the
466 efficiency of reprogramming to *Insulin*-expressing cells is potentiated by forced expression of

467 Pdx1 (Cigliola et al., 2018; Perez-Frances et al., 2021). Thus, the expression of *pdx1* could
468 underlie the intrinsic competence of *sst1.1* δ -cells (or mammalian δ -cells) to induce *ins*.
469 However, *pdx1* expression alone is obviously not sufficient to guarantee *ins* expression, and
470 other mechanisms consequent to β -cell loss must operate in synergy, such as metabolic
471 changes and epigenetic regulations. In contrast to *pdx1*, *nkx6.2* and *mnx1*, two genes essential
472 for β -cell development in zebrafish (A-C Binot et al., 2010; Dalgin et al., 2011), are totally
473 absent in bihormonal cells (Figure 3 and Figure 3-Source data 1). In mammals, the
474 homologue of *nkx6.2* in β -cells is *Nkx6.1*, (see species-specific expression in Figure 3-figure
475 supplement 2). Both *Nkx6.1* and *Mnx1* genes in mouse are important to repress non- β
476 endocrine lineage programs (Pan, Brissova, Powers, Pfaff, & Wright, 2015; Schaffer et al.,
477 2013). Together, the robust expression of *pdx1* and the lack of *mnx1* and *nkx6.2* are potential
478 key players in the hybrid β/δ phenotype.

479 Normal glycemia is nearly recovered after 20 days and regenerated animals display perfectly
480 normal glucose tolerance despite the very low abundance of genuine monohormonal β -cells.
481 Bihormonal cells formed after β -cell destruction are abundant - nearly half the initial β -cell
482 mass - and constitute the vast majority of *ins*-expressing cells throughout the whole pancreas
483 and hence the main source of Ins. Their capacity to regulate blood glucose levels is
484 corroborated by their transcriptomic profile showing the expression of the machinery required
485 for glucose responsiveness and insulin secretion as illustrated by the glucose transporter Glut2
486 (*slc2a2*), the prohormone convertase *pcsk1*, the K_{ATP} subunit SUR1 (*abcc8*) and several
487 components of the secretory pathway. All these findings are further supported by the
488 observation by Singh et al that β/δ hybrid cells gain glucose responsiveness during
489 regeneration as assessed by *in vivo* Calcium imaging (Singh et al., 2021). Altogether, we
490 propose that, despite the fact that bihormonal cells are not identical to β -cells, they are the

491 functional units that control glucose homeostasis in regenerated fish, compensate for the
 492 absence of monohormonal β -cells and reverse diabetes.

493

494

495 **Materials and Methods**

496 *Key resources table*

Reagent type or resource	Designation	Source or reference	Identifier	Additional information
Genetic reagent (Danio rerio)	<i>TgBAC(nkx6.1:eGFP)^{ulg004}</i>	PMID: 26329351	ZFIN: ZDB-ALT-160205-1	
Genetic reagent (Danio rerio)	<i>Tg(ins:NTR-P2A-mCherry)^{ulg034}</i>	PMID: 29663654	ZFIN: ZDB-ALT-171122-9	
Genetic reagent (Danio rerio)	<i>Tg(sst1.1:eGFP)^{ulg054}</i>	This paper		See Zebrafish husbandry and generation of the <i>Tg(sst1.1:eGFP)^{ulg054} zebrafish line</i>
Antibody	Anti-GFP (chicken polyclonal)	Aves Labs	GFP-1020	(1:500)
Antibody	Anti-Insulin (guinea pig polyclonal)	Dako	A0564	(1:500)
Antibody	anti-mCherry/dsRed (Living Colors Polyclonal)	Clontech	632496	(1:500)
Antibody	anti-Pan-RCFP (Living Colors Polyclonal)	Clontech	632475	(1:500)
Antibody	anti-Somatostatin (rat polyclonal)	Invitrogen	MA5-16987	(1:300)
Antibody	anti-Somatostatin (rabbit polyclonal)	Dako	A0566	(1:300)
Antibody	anti-Glucagon (mouse monoclonal)	Sigma	G2654	(1:300)
Antibody	anti-Urocortin 3 (rabbit polyclonal)	Phoenix Pharmaceuticals	H-019-29	(1:300)
Antibody	Anti-Pdx1 (guinea pig polyclonal)	From Chris Wright		(1:200)
Antibody	PCNA	Sigma-Aldrich	P8825	(1:500)
Antibody	Goat anti-Rat IgG (H+L) Cross-Adsorbed, Alexa Fluor™ 488	Invitrogen	A11006	(1:750)
Antibody	Goat anti-Chicken IgY	Invitrogen	A-11039	

	(H+L), Alexa Fluor™ 488			(1:750)
Antibody	Goat anti-Chicken IgY (H+L), Alexa Fluor™ 568	Invitrogen	A-11041	(1:750)
Antibody	Goat anti-Mouse IgG (H+L) Cross-Adsorbed Secondary Antibody, Alexa Fluor 488	Invitrogen	A-11001	(1:750)
Recombinant DNA reagent	p3E-CRE ^{ERT2}	This paper		plasmid
Recombinant DNA reagent	p5E-MCS	Tol2kit	228	plasmid
Recombinant DNA reagent	p3E-eGFP	Tol2kit	366	plasmid
Recombinant DNA reagent	pDestTol2p2A	Tol2kit	394	plasmid
Recombinant DNA reagent	pDONRP2R-P3			plasmid
Sequence- based reagent	O99	This article	PCR primer	GGGGACAGCTTTCTTGTA CAAAGTGG CTGCTAACCATGTTTCATG CCTTC
Recombinant DNA reagent	<i>Tg(ubb:loxP-CFP-loxP- zsYellow)</i>	PMID: 21623370	ZDB- TGCONST RCT- 111115-6	
Sequence- based reagent	O100	This article	PCR primer	GGGGACAACCTTTGTATAA TAAAGTTGTCAAGCTGTG GCAGGGAAACCC
Sequence- based reagent	IM217	This article	PCR primer	TTTTATTAAAGTGTTTATT TGGTCTCAGAG
Sequence- based reagent	IM256	This article	PCR primer	AAGAGCACTTCAGATGTC TTCCC
Sequence- based reagent	O097	This article	PCR primer	GTATCTATAGTTGAACAT GAAAGCAT
Sequence- based reagent	O098	This article	PCR primer	GGTCACACTGACACAAAC AC ACA
Sequence- based reagent	pCR™8/GW/TOPO™	Invitrogen	K250020	
Commercial assay or kit	Gateway™ LR Clonase™ II Enzyme mix	Invitrogen	11791020	
Commercial assay or kit	Gateway™ BP Clonase™ II Enzyme mix	Invitrogen	11789020	
Commercial assay or kit	Nextera® XT DNA Library kit	Illumina	FC-131- 1024	
Commercial	Click-iT™ Edu Cell	Invitrogen	C10340	

assay or kit	Proliferation Kit for Imaging, Alexa Fluor™ 647 dye			
Chemical compound, drug	4-Hydroxytamoxifen	Sigma-Aldrich	H7904	
Chemical compound, drug	Nifurpirinol	Sigma-Aldrich	32439	
Software, algorithm	Flowing Software 2	https://bioscience.fi/services/cell-imaging/flowing-software/	RRID:SCR_015781	Version 2.5.1
Software, algorithm	Imaris	Bitplane (http://www.bitplane.com/imaris/imaris)	RRID:SCR_007370	Version 9.5
Software, algorithm	GraphPad Prism	GraphPad Prism (https://graphpad.com)	RRID:SCR_015807	Version 8
Software, algorithm	DESeq2	DESeq2 (https://bioconductor.org/packages/release/bioc/html/DESeq2.html)	RRID:SCR_015687	
Software, algorithm	WebGestalt	WebGestalt (http://www.webgestalt.org/)	RRID:SCR_006786	

497

498

499 *Zebrafish husbandry and generation of the $Tg(sst1.1:eGFP)^{ulg054}$ zebrafish line*

500 Zebrafish wild-type AB were used in all the experiments. $TgBAC(nkx6.1:eGFP)^{ulg004}$ (Ghaye

501 et al., 2015) and $Tg(ins:NTR-P2A-mCherry)^{ulg034}$ (Bergemann et al., 2018) were used.

502 Zebrafish were raised in standard conditions at 28°C. All experiments were carried out in

503 compliance with the European Union and Belgian law and with the approval of the ULiège

504 Ethical Committee for experiments with laboratory animals (approval numbers 14-1662, 16-

505 1872; 19-2083, 21-2353).

506 To generate the $Tg(sst1.1:eGFP)^{ulg054}$ zebrafish line, the *sst1.1:eGFP* transgene has been

507 generated by cloning a 770 pb PCR fragment containing the *sst1.1* regulatory regions just

508 upstream the ATG of the *sst1.1* ORF (ENSDARG00000040799.4) amplified with primers
509 IM217 (reverse: 5'-TTTTATTAAAGTGTTTATTTGGTCTCAGAG-3') and IM256
510 (forward: 5'-AAGAGCACTTCAGATGTCTTCCC-3') into the Gateway vector
511 pCR8/GW/TOPO. The promoter was assembled by LR recombination with p5E-MCS and
512 p3E-eGFP into pDestTol2p2A from the Tol2kit (Kwan et al., 2007). *Tg(sst1.1:eGFP)^{ulg054}*
513 fish have been generated using the Tol2 mediated transgenesis (Kawakami, 2007). Adult
514 *Tg(sst1.1:eGFP)^{ulg054}* fish (abbreviated *Tg(sst1.1:eGFP)*) were crossed with *Tg(ins:NTR-P2A-*
515 *mCherry)^{ulg034}* to generate a double transgenic line. The *insbglob:loxP-mCherry-nls-loxP-*
516 *DTA* construct was created by cloning a *loxP-mCherry-nls loxP* cassette downstream of the
517 *ins* promoter beta-globin intron (Ninov et al., 2013). Subsequently, a *DTA* gene was cloned
518 downstream of the last *loxP* site via ligation independent cloning (InFusion, Clontech). The
519 *Tg(ins.bglob:loxP-NLS-mCherry-loxP-DTA)^{bns525}* line (abbreviated *Tg(ins:lox-mCherry-lox-*
520 *DTA)*) was generated using the Tol2 system (Kawakami, 2007). The *Tg(ins:CRE-ERT2)* has
521 been generated by LR recombination combining p5E-MCS (Kwan et al., 2007), pME-*ins* and
522 p3E-CRE^{ERT2} vectors into pDestTol2p2A from the Tol2kit. pME-*ins* was obtained by cloning
523 into the pCR8/GW/TOPO a PCR fragment of 897 pb using the primers O097
524 (GTATCTATAGTTGAACATGAAAGCAT) et O098 (GGTCACACTGACACAAACAC
525 ACA) and which contains 744 bp of the insulin promoter, the exon 1 (47 bp), the intron 1 (99
526 bp) and the 7 bp of exon 2 just upstream of the ATG. p3E-CRE^{ERT2} was obtained by BP
527 cloning into the pDONRP2R-P3 the 2200bp PCR fragment using the primers O99
528 GGGGACAGCTTTCTTGTACAAAGTGG CTGCTAACCATGTTTCATGCCTTC and O100
529 GGGGACAACCTTTGTATAATAAAGTTGTCAAGCTGTGGCAGGGAAACCC and as
530 template the pCRE^{ERT2} kindly received from P. Chambon (Feil, Wagner, Metzger, &
531 Chambon, 1997).

532

533 *β-cell ablation*

534 Nifurpirinol (NFP) (32439, Sigma-Aldrich) stock solution was dissolved at 2.5 mM in
535 DMSO. 4-Hydroxytamoxifen (4-OHT, H7904, Sigma-Aldrich) was dissolved in DMSO as a
536 concentrated solution of 10 mM and kept as single-use aliquots at -80°C . β -cell ablation in
537 *Tg(sst1.1:eGFP); Tg(ins:NTR-P2A-mCherry)* larvae was induced by treatment with 4 μM
538 NFP in E3 egg water. Adult fish were treated in fish water with 2.5 μM NFP. Control
539 treatments consisted of E3 containing 0.16% DMSO. Larvae and adults were treated for 18
540 hours in the dark.

541 To induce β -cell ablation with *Tg(ins:lox-mCherry-lox-DTA); Tg(ins:CRE-ERT2)* line, larvae
542 were treated at 7 dpf with 5 μM 4-OHT at in the dark during 2x 2 hours with replacement
543 with fresh 4-OHT. Larvae were then washed several times with E3 egg water to eliminate 4-
544 OHT and allowed to regenerate.

545

546 *β-cell tracing in larvae*

547 β -cell labelling was performed in *Tg(ins:CRE-ERT2); Tg(ubb:loxP-CFP-loxP-zsYellow);*
548 *Tg(sst1.1:GFP); Tg(ins:NTR-P2A-mCherry)* larvae at 6 dpf by 2x2 hours 5 μM 4-OHT before
549 several washes in E3 egg water. At 7 dpf, β -cells were ablated with NFP and larvae were
550 allowed to regenerate until 14 dpf before fixation.

551

552 *Intraperitoneal glucose tolerance test and blood glucose measurements*

553 Adult fish were fasted for 24 hours then euthanized with tricaine and the glycemia was
554 immediately measured using the Accu-Chek Aviva glucometer (Roche Diagnostics) with
555 blood collected at the tail.

556 D-Glucose was dissolved in PBS at 0.5mg/μl. After anaesthesia, adult fish were injected
557 intraperitoneally at 1mg/g fish weight with tricaine as described in (Eames, Philipson, Prince,
558 & Kinkel, 2010).

559

560 *5-ethynyl-2'-deoxyuridine (EdU) incorporation assay*

561 Zebrafish larvae were incubated in 4 mM EdU dissolved in fish E3 water for two day, with
562 replacement of the solution after 24 hours, the were euthanised in tricaine and fixed in 4%
563 PFA. EdU was detected according to the protocol of Click-iT™ EdU Cell Proliferation Kit for
564 Imaging, Alexa Fluor™ 647 (ThermoFisher C10340) and processed for whole mount
565 immunodetection.

566

567 *Immunodetection of paraffin sections*

568 Samples were fixed and processed for immunofluorescence as previously described (Ghaye et
569 al., 2015).

570

571 *Whole mount immunodetection*

572 Larvae were euthanized in tricaine and fixed in 4% PFA at 4 °C for 24 hrs before IHC. After
573 depigmentation with 3% H₂O₂/1% KOH during 15 min, larvae were permeabilised 30 min in
574 PBS/0.5% Triton X-100 and incubated for two hours in blocking buffer (4% goat serum/1%
575 BSA/PBS/0.1% Triton X-100). Primary and secondary antibodies were incubated at 4 °C
576 overnight. Adult fish (6-10 months) were euthanized and fixed for 48 hrs. Digestive tracts
577 were dissected, dehydrated and stored in 100% methanol at -20 °C. Before IHC, the samples
578 were permeabilised in methanol at room temperature for 30 min, placed 1 hr at -80 °C then

579 back at room temperature. After rehydration in PBS/0.05% Triton X-100, depigmentation was
580 performed for 15 min followed by incubation in blocking buffer containing 4% goat serum
581 /1% BSA/PBS/0.01% Triton X-100. The primary antibodies were incubated for 48 hrs on
582 adult samples and overnight on larvae, followed by overnight incubation with the secondary
583 antibodies overnight at 4 °C. Primary antibodies: Anti-Insulin (guinea pig, 1:500, Dako
584 A0564), Living Colors Polyclonal anti-mCherry/dsRed (rabbit, 1:500, Clontech 632496),
585 Living Colors Polyclonal anti-Pan-RCFP (rabbit, 1:500, Clontech 632475), anti-GFP
586 (chicken, 1:1000, Aves lab GFP-1020), anti-Somatostatin (rat, 1:300, Invitrogen MA5-
587 16987), anti-Somatostatin (rabbit, 1:300, Dako, A0566), anti-Glucagon (mouse, 1:300, Sigma
588 G2654), anti-Urocortin 3 (rabbit, 1:300, Phoenix Pharmaceuticals H-019-29), anti-Pdx1
589 (guinea pig, 1:200, kind gift from Chris Wright, Vanderbilt University), anti-PCNA (clone
590 PC10 Sigma P8825). Secondary antibodies: Alexa Fluor-488, -568, -633 (goat, 1:750,
591 Molecular Probes).

592

593 *Whole mount in situ hybridization on embryos*

594 The *sst1.1* and *sst2* probes were described in (Devos et al., 2002). The *ins* probe has been
595 described in (Milewski, Duguay, Chan, & Steiner, 1998). Fluorescent in situ hybridization
596 were performed as described in (Tarifeño-Saldivia et al., 2017) on 3 or 6 days post
597 fertilization embryos (dpf). The antisense RNA probes were revealed using tyramide-Cy3
598 followed by immunodetection of GFP.

599 Images of immunodetection and in *situ* hybridization were acquired with a Leica SP5 or a
600 Zeiss LSM880 confocal microscope, and processed with Imaris 9.5 (Bitplane) for
601 visualization.

602

603 *In vivo imaging*

604 *In vivo* imaging was performed with a Lightsheet Zeiss Z1 microscope using a 20x water
605 immersion objective and 488nm and 561nm lasers. *Tg(sst1.1:eGFP); Tg(ins:NTR-P2A-*
606 *mCherry)* larvae were treated from 1 dpf with 1-phenyl 2-thiourea (0.003% (w:v)) to inhibit
607 pigment synthesis. After ablation with NFP from 3 to 4 dpf, larvae were anesthetized,
608 embedded in 0.25% low melting agarose containing and mounted into FEP capillaries. Images
609 were acquired every 30 min and were maintained during the whole experiment at 28° and
610 with 100 ml/L tricaine. Images were converted with Imaris 9.5 (Bitplane) for visualization.

611

612 *Flow cytometry and FACS*

613 The zebrafish pancreas contains one main big islet in the head and several smaller secondary
614 islets in the tail. The main islets from 2-4 pancreata of *Tg(sst1.1:eGFP); Tg(ins:NTR-P2A-*
615 *mCherry)* adult fish (6–10 months old, males and females) were dissected under
616 epifluorescence to eliminate a maximum of non-fluorescent surrounding exocrine tissue,
617 collected and washed in HBSS without $\text{Ca}^{2+}/\text{Mg}^{2+}$. Live cell dissociation was performed in
618 Tryple Select 1x solution (GIBCO) supplemented with 100 U/mL collagenase IV (Life
619 Technologies 17104-019) and 40 $\mu\text{g}/\text{mL}$ proteinase K (Invitrogen, 25530031) for 10 min at
620 28 °C, and stopped with 15% FBS. The GFP+ cells, mCherry+ cell and double GFP+
621 mCherry+ cells were selected according to gates as shown in Figure 1-figure supplement 2
622 (dashed lines) on FACS Aria III and sorted under purity mode and after exclusion of the
623 doublets. The purity of the sorted cells was confirmed by epifluorescence microscopy (~95
624 %). Cells (about 1000-5000/fish depending on the cell type) were immediately lysed with
625 0.5% Triton X-100 containing 2U/ μl RNase inhibitor and stored at –80 °C. Similar strategy
626 was followed for cell quantification in secondary islets present in the pancreatic tail. The

627 pancreas was dissected excluding the anterior most part containing the main islet and whole
628 posterior tissues were dissociated and analysed.

629

630 *Cell quantification in adults by flow cytometry*

631 The percentage of mCherry⁺, GFP⁺ and double mCherry⁺ GFP⁺ fluorescent cells in the
632 dissociated islets was inferred from flow cytometry experiments in each quadrant delimiting
633 negative and positive fluorescence. FACS plots were generated by FlowJo 10.6.2 and
634 quantifications were performed using Flowing Software 2.5.1.

635

636 *mRNA sequencing of FACSed cells and bioinformatic analyses*

637 cDNAs were prepared from lysed cells according to SMART-Seq2.0 (Picelli et al., 2014) for
638 low input RNA sequencing and libraries were prepared with Nextera® DNA Library kit
639 (Illumina). Independent biological replicates of each cell type sequenced using Illumina
640 HiSeq2500 and obtained ~20 million 75 bp single-end reads (7 replicates for β -cells, 6 for 20
641 dpt bihormonal cells, 3 for sst1.1GFP^{high}, 3 for sst1.1GFP^{low}). Reads were mapped and aligned
642 to the zebrafish genome GRCz11 from Ensembl gene annotation version 92 using STAR
643 (Dobin et al., 2013). Gene expression levels were calculated with featureCounts
644 (<http://bioinf.wehi.edu.au/featureCounts/>) and differential expression determined with
645 DESeq2 (Love, Huber, & Anders, 2014). Expression values are given as normalized read
646 counts. Poorly expressed genes with mean normalized expression counts <10 were excluded
647 from the subsequent analyses. DESeq2 uses Wald test for significance with posterior
648 adjustment of P values (P_{adj}) using Benjamini and Hochberg multiple testing. The
649 differentially expressed (DE) genes identified with a P_{adj} cutoff of 0.05 and fold change

650 above 2 were submitted for GO analysis using WebGestalt tool (Liao, Wang, Jaehnig, Shi, &
651 Zhang, 2019).

652 The genes enriched in β -cells and *sst2* δ -cells above 4-fold were identified using sequences
653 obtained previously (Tarifeño-Saldivia et al., 2017) with prior mapping on the more recent
654 GRCz11 v92 assembly of the zebrafish genome; they thus slightly differ from the gene list
655 previously published (provided in Figure 3-Source Data 2). Then, new enrichment was
656 updated to take into account the new transcriptomic data obtained for *sst1.1* δ -cells from
657 *Tg(sst1.1:eGFP)* and the new β -cells from *Tg(ins:NTR-P2A-mCherry)* (presented in Figure 4-
658 Source Data 3).

659

660 *Statistical analyses*

661 Graphs and statistical analyses were performed using GraphPad Prism 8. Data are represented
662 as Mean \pm SD except in Figure 4C where Mean \pm SEM are shown. The statistical tests are
663 described in the legend of the Figures.

664

665 **Acknowledgments**

666 The authors thank the GIGA technology platforms GIGA-Zebrafish, GIGA-Genomics and
667 GIGA-Imaging. The authors also thanks Chris Wright for providing the Pdx1 antibody.

668

669 **Duality of Interest**

670 No potential conflicts of interest.

671 **References**

- 672 Ahlgren, U., Jonsson, J., Jonsson, L., Simu, K., & Edlund, H. (1998). beta-cell-specific
673 inactivation of the mouse *Ipf1/Pdx1* gene results in loss of the beta-cell phenotype and
674 maturity onset diabetes. *Genes & Development*, *12*(12), 1763–1768.
675 <https://doi.org/10.1101/gad.12.12.1763>
- 676 Bergemann, D., Massoz, L., Bourdouxhe, J., Carril Pardo, C. A., Voz, M. L., Peers, B., &
677 Manfroid, I. (2018). Nifurpirinol: A more potent and reliable substrate compared to
678 metronidazole for nitroreductase-mediated cell ablations. *Wound Repair and*
679 *Regeneration : Official Publication of the Wound Healing Society [and] the European*
680 *Tissue Repair Society*. <https://doi.org/10.1111/wrr.12633>
- 681 Binot, A-C, Manfroid, I., Flasse, L., Winandy, M., Motte, P., Martial, J. A., ... Voz, M. L.
682 (2010). Nkx6.1 and nkx6.2 regulate alpha- and beta-cell formation in zebrafish by acting
683 on pancreatic endocrine progenitor cells. *Developmental Biology*, *340*(2), 397–407.
684 <https://doi.org/10.1016/j.ydbio.2010.01.025>
- 685 Binot, A.-C., Manfroid, I., Flasse, L., Winandy, M., Motte, P., Martial, J. A., ... Voz, M. L.
686 (2010). Nkx6.1 and nkx6.2 regulate α - and β -cell formation in zebrafish by acting on
687 pancreatic endocrine progenitor cells. *Developmental Biology*, *340*(2).
688 <https://doi.org/10.1016/j.ydbio.2010.01.025>
- 689 Blum, B., Hrvatin, S., Schuetz, C., Bonal, C., Rezanian, A., & Melton, D. A. (2012).
690 Functional beta-cell maturation is marked by an increased glucose threshold and by
691 expression of urocortin 3. *Nature Biotechnology*, *30*(3), 261–264.
692 <https://doi.org/10.1038/nbt.2141>
- 693 Chera, S., Baronnier, D., Ghila, L., Cigliola, V., Jensen, J. N., Gu, G., ... Herrera, P. L.

694 (2014). Diabetes recovery by age-dependent conversion of pancreatic delta-cells into
695 insulin producers. *Nature*, *514*(7523), 503–507. <https://doi.org/10.1038/nature13633>

696 Cigliola, V., Ghila, L., Thorel, F., van Gurp, L., Baronnier, D., Oropeza, D., ... Herrera, P. L.
697 (2018). Pancreatic islet-autonomous insulin and smoothed-mediated signalling
698 modulate identity changes of glucagon(+) α -cells. *Nature Cell Biology*, *20*(11), 1267–
699 1277. <https://doi.org/10.1038/s41556-018-0216-y>

700 Curado, S., Anderson, R. M., Jungblut, B., Mumm, J., Schroeter, E., & Stainier, D. Y. R.
701 (2007). Conditional targeted cell ablation in zebrafish: a new tool for regeneration
702 studies. *Developmental Dynamics : An Official Publication of the American Association*
703 *of Anatomists*, *236*(4), 1025–1035. <https://doi.org/10.1002/dvdy.21100>

704 Dalgin, G., Ward, A. B., Hao, L. T., Beattie, C. E., Nechiporuk, A., & Prince, V. E. (2011).
705 Zebrafish *mxn1* controls cell fate choice in the developing endocrine pancreas.
706 *Development (Cambridge, England)*, *138*(21), 4597–4608.
707 <https://doi.org/10.1242/dev.067736>

708 Delaspre, F., Beer, R. L., Rovira, M., Huang, W., Wang, G., Gee, S., ... Parsons, M. J.
709 (2015). Centroacinar Cells Are Progenitors That Contribute to Endocrine Pancreas
710 Regeneration. *Diabetes*, *64*(10), 3499–3509. <https://doi.org/10.2337/db15-0153>

711 Devos, N., Deflorian, G., Biemar, F., Bortolussi, M., Martial, J. A., Peers, B., & Argenton, F.
712 (2002). Differential expression of two somatostatin genes during zebrafish embryonic
713 development. *Mechanisms of Development*, *115*(1–2), 133–137.
714 [https://doi.org/10.1016/s0925-4773\(02\)00082-5](https://doi.org/10.1016/s0925-4773(02)00082-5)

715 Dobin, A., Davis, C. A., Schlesinger, F., Drenkow, J., Zaleski, C., Jha, S., ... Gingeras, T. R.
716 (2013). STAR: ultrafast universal RNA-seq aligner. *Bioinformatics (Oxford, England)*,
717 *29*(1), 15–21. <https://doi.org/10.1093/bioinformatics/bts635>

718 Eames, S. C., Philipson, L. H., Prince, V. E., & Kinkel, M. D. (2010). Blood sugar
719 measurement in zebrafish reveals dynamics of glucose homeostasis. *Zebrafish*, 7(2),
720 205–213. <https://doi.org/10.1089/zeb.2009.0640>

721 Feil, R., Wagner, J., Metzger, D., & Chambon, P. (1997). Regulation of Cre recombinase
722 activity by mutated estrogen receptor ligand-binding domains. *Biochemical and*
723 *Biophysical Research Communications*, 237(3), 752–757.
724 <https://doi.org/10.1006/bbrc.1997.7124>

725 Gao, T., McKenna, B., Li, C., Reichert, M., Nguyen, J., Singh, T., ... Stanger, B. Z. (2014).
726 Pdx1 maintains β cell identity and function by repressing an α cell program. *Cell*
727 *Metabolism*, 19(2), 259–271. <https://doi.org/10.1016/j.cmet.2013.12.002>

728 Ghaye, A. P., Bergemann, D., Tarifeño-Saldivia, E., Flasse, L. C., Von Berg, V., Peers, B., ...
729 Manfroid, I. (2015). Progenitor potential of nkx6.1-expressing cells throughout zebrafish
730 life and during beta cell regeneration. *BMC Biology*, 13(1).
731 <https://doi.org/10.1186/s12915-015-0179-4>

732 Hans, S., Kaslin, J., Freudenreich, D., & Brand, M. (2009). Temporally-controlled site-
733 specific recombination in zebrafish. *PloS One*, 4(2), e4640.
734 <https://doi.org/10.1371/journal.pone.0004640>

735 Kawakami, K. (2007). Tol2: a versatile gene transfer vector in vertebrates. *Genome Biology*, 8
736 *Suppl 1*, S7. <https://doi.org/10.1186/gb-2007-8-s1-s7>

737 Kwan, K. M., Fujimoto, E., Grabher, C., Mangum, B. D., Hardy, M. E., Campbell, D. S., ...
738 Chien, C.-B. (2007). The Tol2kit: a multisite gateway-based construction kit for Tol2
739 transposon transgenesis constructs. *Developmental Dynamics : An Official Publication*
740 *of the American Association of Anatomists*, 236(11), 3088–3099.
741 <https://doi.org/10.1002/dvdy.21343>

742 Leonard, J., Peers, B., Johnson, T., Ferreri, K., Lee, S., & Montminy, M. R. (1993).
743 Characterization of somatostatin transactivating factor-1, a novel homeobox factor that
744 stimulates somatostatin expression in pancreatic islet cells. *Molecular Endocrinology*
745 (*Baltimore, Md.*), 7(10), 1275–1283. <https://doi.org/10.1210/mend.7.10.7505393>

746 Liao, Y., Wang, J., Jaehnig, E. J., Shi, Z., & Zhang, B. (2019). WebGestalt 2019: gene set
747 analysis toolkit with revamped UIs and APIs. *Nucleic Acids Research*, 47(W1), W199–
748 W205. <https://doi.org/10.1093/nar/gkz401>

749 Love, M. I., Huber, W., & Anders, S. (2014). Moderated estimation of fold change and
750 dispersion for RNA-seq data with DESeq2. *Genome Biology*, 15(12), 550.
751 <https://doi.org/10.1186/s13059-014-0550-8>

752 Milewski, W. M., Duguay, S. J., Chan, S. J., & Steiner, D. F. (1998). Conservation of PDX-1
753 structure, function, and expression in zebrafish. *Endocrinology*, 139(3), 1440–1449.
754 <https://doi.org/10.1210/endo.139.3.5768>

755 Moin, A. S. M., & Butler, A. E. (2019). Alterations in Beta Cell Identity in Type 1 and Type 2
756 Diabetes. *Current Diabetes Reports*, 19(9), 83. [https://doi.org/10.1007/s11892-019-](https://doi.org/10.1007/s11892-019-1194-6)
757 [1194-6](https://doi.org/10.1007/s11892-019-1194-6)

758 Mosimann, C., Kaufman, C. K., Li, P., Pugach, E. K., Tamplin, O. J., & Zon, L. I. (2011).
759 Ubiquitous transgene expression and Cre-based recombination driven by the ubiquitin
760 promoter in zebrafish. *Development (Cambridge, England)*, 138(1), 169–177.
761 <https://doi.org/10.1242/dev.059345>

762 Moss, J. B., Koustubhan, P., Greenman, M., Parsons, M. J., Walter, I., & Moss, L. G. (2009).
763 Regeneration of the pancreas in adult zebrafish. *Diabetes*, 58(8), 1844–1851.
764 <https://doi.org/10.2337/db08-0628>

765 Ninov, N., Hesselton, D., Gut, P., Zhou, A., Fidelin, K., & Stainier, D. Y. R. (2013).
766 Metabolic regulation of cellular plasticity in the pancreas. *Current Biology : CB*, 23(13),
767 1242–1250. <https://doi.org/10.1016/j.cub.2013.05.037>

768 Pan, F. C., Brissova, M., Powers, A. C., Pfaff, S., & Wright, C. V. E. (2015). Inactivating the
769 permanent neonatal diabetes gene *Mnx1* switches insulin-producing β -cells to a δ -like
770 fate and reveals a facultative proliferative capacity in aged β -cells. *Development*
771 (*Cambridge, England*), 142(21), 3637–3648. <https://doi.org/10.1242/dev.126011>

772 Parsons, M. J., Pisharath, H., Yusuff, S., Moore, J. C., Siekmann, A. F., Lawson, N., & Leach,
773 S. D. (2009). Notch-responsive cells initiate the secondary transition in larval zebrafish
774 pancreas. *Mechanisms of Development*, 126(10), 898–912.
775 <https://doi.org/10.1016/j.mod.2009.07.002>

776 Perez-Frances, M., van Gurp, L., Abate, M. V., Cigliola, V., Furuyama, K., Bru-Tari, E., ...
777 Herrera, P. L. (2021). Pancreatic Ppy-expressing γ -cells display mixed phenotypic traits
778 and the adaptive plasticity to engage insulin production. *Nature Communications*, 12(1),
779 4458. <https://doi.org/10.1038/s41467-021-24788-0>

780 Picelli, S., Faridani, O. R., Björklund, A. K., Winberg, G., Sagasser, S., & Sandberg, R.
781 (2014). Full-length RNA-seq from single cells using Smart-seq2. *Nature Protocols*, 9(1),
782 171–181. <https://doi.org/10.1038/nprot.2014.006>

783 Piran, R., Lee, S.-H., Li, C.-R., Charbono, A., Bradley, L. M., & Levine, F. (2014).
784 Pharmacological induction of pancreatic islet cell transdifferentiation: relevance to type
785 I diabetes. *Cell Death & Disease*, 5(7), e1357. <https://doi.org/10.1038/cddis.2014.311>

786 Pisharath, H., & Parsons, M. J. (2009). Nitroreductase-mediated cell ablation in transgenic
787 zebrafish embryos. *Methods in Molecular Biology (Clifton, N.J.)*, 546, 133–143.
788 https://doi.org/10.1007/978-1-60327-977-2_9

789 Schaffer, A. E., Taylor, B. L., Benthuyssen, J. R., Liu, J., Thorel, F., Yuan, W., ... Sander, M.
790 (2013). Nkx6.1 controls a gene regulatory network required for establishing and
791 maintaining pancreatic Beta cell identity. *PLoS Genetics*, 9(1), e1003274.
792 <https://doi.org/10.1371/journal.pgen.1003274>

793 Segerstolpe, A., Palasantza, A., Eliasson, P., Andersson, E.-M., Andreasson, A.-C., Sun, X.,
794 ... Sandberg, R. (2016). Single-Cell Transcriptome Profiling of Human Pancreatic Islets
795 in Health and Type 2 Diabetes. *Cell Metabolism*, 24(4), 593–607.
796 <https://doi.org/10.1016/j.cmet.2016.08.020>

797 Singh, S. P., Chawla, P., Hnatiuk, A., Kamel, M., Silva, L. D., Spanjard, B., ... Ninov, N.
798 (2021). A single-cell atlas of de novo β -cell regeneration reveals
799 the contribution of hybrid β/δ cells to diabetes recovery in zebrafish. *BioRxiv*,
800 2021.06.24.449704. <https://doi.org/10.1101/2021.06.24.449704>

801 Singh, S. P., Janjuha, S., Hartmann, T., Kayisoglu, O., Konantz, J., Birke, S., ... Ninov, N.
802 (2017). Different developmental histories of beta-cells generate functional and
803 proliferative heterogeneity during islet growth. *Nature Communications*, 8(1), 664.
804 <https://doi.org/10.1038/s41467-017-00461-3>

805 Spanjaard, B., Hu, B., Mitic, N., Olivares-Chauvet, P., Janjuha, S., Ninov, N., & Junker, J. P.
806 (2018). Simultaneous lineage tracing and cell-type identification using CRISPR-Cas9-
807 induced genetic scars. *Nature Biotechnology*, 36(5), 469–473.
808 <https://doi.org/10.1038/nbt.4124>

809 Tarifeño-Saldivia, E., Lavergne, A., Bernard, A., Padamata, K., Bergemann, D., Voz, M. L.,
810 ... Peers, B. (2017). Transcriptome analysis of pancreatic cells across distant species
811 highlights novel important regulator genes. *BMC Biology*, 15(1).
812 <https://doi.org/10.1186/s12915-017-0362-x>

813 Thorel, F., Nepote, V., Avril, I., Kohno, K., Desgraz, R., Chera, S., & Herrera, P. L. (2010).
814 Conversion of adult pancreatic alpha-cells to beta-cells after extreme beta-cell loss.
815 *Nature*, 464(7292), 1149–1154. <https://doi.org/10.1038/nature08894>

816 Waeber, G., Thompson, N., Nicod, P., & Bonny, C. (1996). Transcriptional activation of the
817 GLUT2 gene by the IPF-1/STF-1/IDX-1 homeobox factor. *Molecular Endocrinology*
818 (*Baltimore, Md.*), 10(11), 1327–1334. <https://doi.org/10.1210/mend.10.11.8923459>

819 Wang, Y., Rovira, M., Yusuff, S., & Parsons, M. J. (2011). Genetic inducible fate mapping in
820 larval zebrafish reveals origins of adult insulin-producing beta-cells. *Development*
821 (*Cambridge, England*), 138(4), 609–617. <https://doi.org/10.1242/dev.059097>

822 Watada, H., Kajimoto, Y., Miyagawa, J., Hanafusa, T., Hamaguchi, K., Matsuoka, T., ...
823 Yamasaki, Y. (1996). PDX-1 induces insulin and glucokinase gene expressions in
824 alphaTC1 clone 6 cells in the presence of betacellulin. *Diabetes*, 45(12), 1826–1831.
825 <https://doi.org/10.2337/diab.45.12.1826>

826 Ye, L., Robertson, M. A., Hesselton, D., Stainier, D. Y. R., & Anderson, R. M. (2015).
827 Glucagon is essential for alpha cell transdifferentiation and beta cell neogenesis.
828 *Development (Cambridge, England)*, 142(8), 1407–1417.
829 <https://doi.org/10.1242/dev.117911>

830

831 **Figure legends**

832 **Figure 1. Most new *ins*⁺ cells after ablation and regeneration in zebrafish are *Ins*⁺**
833 ***Sst1.1*⁺ bihormonal cells**

834 A) Blood glucose level (mg/ml) of adult *Tg(ins:NTR-P2A-mCherry)* control fish (CTL, 66 ±
835 15 mg/dl), 3 days (510 ± 126 mg/dl) and 20 days post treatment (dpt) (117 ± 29 mg/dl) with
836 the NFP prodrug to trigger β-cell ablation. The huge rise of glycemia at 3 dpt confirms the
837 efficiency of ablation. One-way ANOVA Kruskal-Wallis test (with Dunn's multiple
838 comparisons); Mean ± SD; ***P*<0.005, *****P*<0.0001. (See Figure 1-Source Data 1)

839 B) Immunolabelling of β- and δ-cells with anti-INS (red) and anti-SST (green), respectively,
840 on paraffin sections through the main islet of *Tg(ins:NTR-P2A-mCherry)* adult fish in control
841 condition (CTL) and at 20 dpt. In CTL islet, no appreciable overlap between the two markers
842 can be detected while broad colabelling is observed at 20 dpt and represented by many yellow
843 cells (arrowheads).

844 C) Whole mount immunodetection of β- and *sst1.1*⁺ cells in the main islet of adult
845 *Tg(sst1.1:GFP);Tg(ins:NTR-P2A-mCherry)* fish by labelling with anti-GFP marking *sst1.1*-
846 expressing cells and anti-mCherry for β-cells. Both cell types show no or very few
847 overlapping in CTL fish. At 3 and 20 dpt, many double GFP⁺ mCherry⁺ cells are observed
848 (yellow cells, arrowheads). Bright mCherry⁺ β-cell debris are detectable at 3 dpt (white
849 asterisk).

850 D-G) Quantification of the GFP⁺, mCherry⁺ (β-cells) and double GFP⁺ mCherry⁺ cells
851 detected by FACS in the main islets of *Tg(sst1.1:GFP);Tg(ins:NTR-P2A-mCherry)* CTL fish
852 and following β-cell ablation (3 and 20 dpt), based on fluorescence analysis shown in Figure
853 1-figure supplement 3. D) Total islet cell number in CTL, 3 dpt and 20 dpt islets. E) CTL

854 islets contain 3277 ± 1220 mCherry+ (GFP-) β -cells. At 3 dpt, ablated β -cells represent $105 \pm$
855 70 cells and were even more scarce at 20 dpt (14 cells). F) Double GFP+ mCherry+
856 bihormonal cells represent 135 ± 45 cells in CTL islets, 1411 ± 421 cells at 3 dpt and $1409 \pm$
857 655 cells at 20 dpt. G) GFP+ (mCherry-) cells represent 2833 ± 615 cells in CTL islets. One-
858 way ANOVA Kruskal-Wallis test (with Dunn's multiple comparison); *ns*, not significant,
859 * $P < 0.05$, ** $P < 0.005$, *** $P < 0.0005$, **** $P < 0.0001$; Mean \pm SD (See Figure 1-Source Data
860 2)

861

862 **Figure 2. Bihormonal cell formation is age- and ablation model-independent and mostly**
863 **do not derive from escaping β -cells**

864 A) Whole mount immunodetection in 6 dpf *Tg(ss1.1:GFP); Tg(ins:NTR-P2A-mCherry)*
865 larvae showing β -cells (mCherry, red), *ss1.1*-expressing cells (GFP, green) and double
866 positive bihormonal cells (asterisks) in the main islet in control (CTL) and 3 days after NFP-
867 mediated ablation (3 dpt). Representative confocal images (single optical planes). dpf: days
868 post-fertilization

869 B) Quantification of bihormonal cells co-labelled by mCherry and GFP based on confocal
870 images of 6 dpf larvae. Unpaired two-tailed t-test (with Welch correction); *** $P < 0.001$;
871 Mean \pm SD.

872 C) Whole mount fluorescent *in situ* hybridization performed on 6 dpf *Tg(ins:NTR-P2A-*
873 *mCherry)* larvae with an *ins* antisense RNA probe (green) combined with either a *ss1.1* or a
874 *ss2* probe (red). NFP-mediated ablation was performed from 3 to 4 dpf. Representative
875 confocal images of the main islet (single optical planes).

876 D-G) β -cell tracing with *Tg(ins:CRE-ERT2); Tg(ubb:loxP-CFP-loxP-zsYellow);*
877 *Tg(sst1.1:GFP); Tg(ins:NTR-P2A-mCherry)* larvae. D) Experimental design: CRE
878 recombination was performed by treatment with 4-OHT treatment at 6 dpf to induce the
879 expression of the lineage tracer zsYellow (grey) in β -cells (INS, red). β -cell ablation (NFP)
880 was then performed at 7 dpf and the lineage tracer was analysed in the main islet at 14 dpf (7
881 dpt). E-E') Confocal images showing immunodetection of GFP (green), zsYellow (grey) and
882 INS (red) antibodies. After ablation, traced β -cells are evidenced by double zsYellow+ Ins+
883 staining (grey arrowheads) and bihormonal cells by double Ins+ GFP+ staining (white
884 asterisks). E') Close-up showing two bihormonal cells, one zsYellow+ (derived from a pre-
885 existing β -cell) (yellow arrowhead) and one zsYellow- (asterisk). F-H) Quantification (CTL,
886 n=6; NFP, n=8) based on the confocal images. F) In CTL non-ablated islets, ZsYellow
887 marked efficiently the Ins+ β -cells (84 ± 19 zsYellow+ Ins+ cells out of 89 ± 20 total Ins+ β -
888 cells, representing 94% of the total β -cells). ZsYellow was not detected in *sst1.1:GFP+* cells,
889 showing a good specificity. G) 7 days after ablation (NFP), 47.3 ± 8 Ins+ cells were detected
890 and 5.8 ± 4 of them (12%) expressed zsYellow. H) 42 ± 7.5 Ins+ cells are also GFP+
891 bihormonal and 10% of them (4 ± 3 cells) are labelled with zsYellow. Mean \pm SD.

892

893 **Figure 3. Transcriptomic comparison of bihormonal cells and β -cells**

894 A) Heatmap representation of the transcriptomes of 20 dpt bihormonal (6 replicates) and β -
895 cells (7 replicates) (significant DE genes).

896 B) Volcano plot showing the distribution of genes in β -cells without ablation and bihormonal
897 cells. The x-axis represents the \log_2 of fold change (FC) and the y-axis the \log_{10} of adjusted P
898 value (P_{adj}) provided by DESeq. The red dots highlight the significantly DE genes
899 (P_{adj}<0.05). A full list of significant DE genes is provided in Figure 3-Source Data 1.

900 C) Expression values (mean normalized reads) as provided by DESeq of the main hormones
901 and endocrine genes in β -cell and bihormonal cell transcriptomes. *sst1.1* and *ins* are the two
902 highest expressed hormones. Padj are calculated by DESeq. *ns*: no significant DE between the
903 two conditions, $0.05 < P^* < 0.005$, $0.005 < P^{**} < 0.0005$, $P^{*****} < 0.000005$.

904 D) Heatmap plot showing the direction and amplitude of changes in expression of the β -cell
905 markers between normal β -cells and bihormonal cells (significant DEG only). The 62 β -cell
906 markers are provided in Figure 3-Source Data 2.

907 E) Expression values (mean normalized reads) as provided by DESeq of selected β -cell
908 markers and genes important for β -cell function in β -cells and bihormonal cells. Padj are
909 calculated by DESeq. *ns*: no significant DE between the two conditions, $0.05 < P^* < 0.005$,
910 $0.005 < P^{**} < 0.0005$, $0.00005 < P^{*****} < 0.000005$, $P^{*****} < 0.000005$.

911 F) Enriched Gene Ontology (GO) terms. Top 10 or Padj (FDR) < 0.25 Biological Processes
912 (BP) and KEGG pathways are shown. The plots represent the enrichment ratio of Biological
913 Processes and KEGG pathways identified with WebGestalt (Liao et al., 2019) using the genes
914 over- and underexpressed in bihormonal cells compared to β -cells obtained with a 2-fold
915 differential expression and Padj < 0.05 . All overrepresented Biological Processes and Pathways
916 ($< \text{FDR } 0.25$) are listed in Figure 3-Source Data 3 (bihormonal cells) and Figure 3-Source
917 Data 4 (β -cells).

918 G) Over- and underexpression of selected significantly DE genes from the BP and KEGG
919 pathways identified in β -cells and bihormonal cells (Fold Change, log2 scale).

920

921 **Figure 4. Bihormonal cells are the main source of Insulin in the whole pancreas after**
922 **regeneration and regulate blood glucose homeostasis**

923 A) Whole mount immunofluorescence (GFP and mCherry) on the pancreas of
924 *Tg(sst1.1:eGFP); Tg(ins:NTR-P2A-mCherry)* adult zebrafish showing secondary islets in the
925 pancreatic tail. One representative CTL and two independent 20 dpt samples are shown.
926 Coexpressing cells appear in yellow due to overlapping GFP and mCherry staining. Confocal
927 optical section (Z-planes) and 3D projections (stacks) are shown.

928 B) Quantification of monohormonal mCherry⁺ β -cells and GFP⁺ mCherry⁺ bihormonal cells
929 detected by FACS in the tail of CTL fish and after 20 days regeneration (20 dpt). Mann-
930 Whitney test. $P^{**}=0.0079$ in both graphs. Mean \pm SD. (See also Figure 4-Source Data 1).

931 C) Intraperitoneal glucose tolerance test performed in adult zebrafish. Blood glucose was
932 measured over time in control (non-ablated, DMSO) and NFP-treated (ablated) fish after
933 intraperitoneal injection of 0.5 mg/ μ l of D-Glucose. $4 \leq N \leq 9$ per time point for CTL and
934 NFP. Two-way ANOVA test with Sidak's multiple comparison test. Mean \pm SEM; *ns*: not
935 significant.

936

937 **Figure 5. *sst1.1* δ -cells (GFP^{high}) constitute a δ -cell subpopulation distinct from *sst2* δ -**
938 **cells (GFP^{low}) that presents similarities with β -cells**

939 A) Whole mount immunodetection on t *Tg(sst1.1:eGFP); Tg(ins:NTR-P2A-mCherry)* main
940 islets of GFP (green), mCherry (red) and Sst (gray) revealing two levels of GFP expression
941 (green light and dark arrowheads) that parallel the expression level of Sst. These cells are
942 mCherry negative.

943 B) PCA plot showing the separation between *sst1.1*:GFP^{high} (n=3), *sst1.1*:GFP^{low} (n=3),
944 bihormonal (n=6) and β -cells (n=7) based on their transcriptomic profile. 49% of the variance
945 is explained in PC1. PCA analysis failed to separate bihormonal and *sst1.1*:GFP^{high} cells while

946 separated well β -cells from the *sst1.1:GFP^{low}* cells. The *sst1.1:GFP^{high}*/bihormonal cluster
947 located between β -cells and *sst1.1:GFP^{low}* cells shows that β -cells are more similar to
948 *sst1.1:GFP^{high}*/bihormonal cells.

949 C) Heatmap plot showing the clustering of the *sst1.1:GFP^{high}* and *sst1.1:GFP^{low}* populations,
950 the bihormonal cells, the β -cells of the present study and the previously published data for β -,
951 α - and *sst2* δ -cells (n=3) (Tarifeño-Saldivia et al., 2017). In addition to revealing the expected
952 clustering between both RNAseq data from β -cells (Tarifeño-Saldivia et al., 2017) and this
953 study), this plot also shows the clustering of the *GFP^{low}* cells together with *sst2* δ -cells.

954 D) Volcano plot showing the distribution of genes expressed in *GFP^{high}* and *GFP^{low}*
955 populations. The x-axis represents the \log_2 of fold change (FC) and the y-axis the \log_{10} of
956 adjusted P value (P_{adj}) provided by DESeq. The list of all DE genes is provided in Figure 5-
957 Source Data 1.

958 E) Expression of the main pancreatic hormones in *GFP^{high}* and *GFP^{low}* populations (mean
959 normalized reads). Expression is expressed as normalized counts and P_{adj} are calculated by
960 DESeq. *ns*: no significant DE between the two conditions, $0.05 < * < 0.005$,
961 $0.0005 < *** < 0.00005$.

962 F) Venn diagram showing the overlap between genes overexpressed in *GFP^{low}* cells (versus
963 *GFP^{high}*) and *sst2* δ -cell markers previously identified, and between genes overexpressed in
964 *GFP^{high}* cells (versus *GFP^{low}* cells) and β -cell genes (Figure 5-Source Data 2). Representation
965 factor and P value calculated by Fisher's exact test.

966 G) Expression of selected β - and *sst2* δ -cell genes in each replicate of *GFP^{high}* and *GFP^{low}*
967 cells. *GFP^{high}* cells distinctly express high levels of *sst1.1* and will be referred to as

968 GFP^{high}/*sst1.1* δ -cells, and GFP^{low} to GFP^{low}/*sst2* δ -cells. 0.05<*<0.005, 0.005<***<0.0005,
969 0.0005<***<0.00005, ****<0.00001

970 H) Confocal images showing immunodetection of Pdx1 (anti-Pdx1, red) and Sst (anti-SST,
971 grey) on paraffin section through the main islet of a non-ablated adult fish showing double
972 Pdx1+ Sst+ cells (white arrowheads) and Pdx1- Sst+ cells (yellow arrowheads). Red asterisks
973 highlight Pdx1 single positive cells β -cells.

974 I) Confocal images showing whole mount immunodetection of Ucn3 (red), GFP (green) and
975 Ins (grey) in CTL and 3 dpt main islets from *Tg(sst1.1:eGFP); Tg(ins:NTR-P2A-mCherry)*
976 adult fish. In CTL islets, strong Ucn3 labelling is detected in β -cells as well as in some
977 *sst1.1*:GFP cells (white arrowheads). After β -cell ablation, Ucn3 is principally expressed in
978 GFP+ cells that also harbour faint Ins staining.

979 J) Biological Processes (BP) and KEGG pathways overrepresented in GFP^{high}/*sst1.1* δ -cells
980 (UP) compared to GFP^{low} cells (DOWN) (Padj<0.25). Gene Ontology (GO) terms were
981 identified by WebGestalt (Liao et al., 2019) using the list of DE genes between GFP^{high}/*sst1.1*
982 δ -cells and GFP^{low}/*sst2* δ -cells obtained with at least 2-fold differential expression and
983 Padj<0.05 provided by DESeq. The list of all BP and KEGG pathways below FDR 0.25 is
984 given in Figure 5-Source Data 4 and 5.

985

986 **Figure 6. *sst1.1* δ -cells convert to Sst1.1+ Ins+ bihormonal cells after β -cell destruction**
987 **and activate cell cycle genes and p53.**

988 A) Quantification by flow cytometry of GFP^{high}/*sst1.1* δ -cells before ablation (CTL) and at 3
989 and 20 dpt showing depletion of *sst1.1* δ -cells during regeneration. Cells were isolated from

990 dissected main islets of adult *Tg(sst1.1:eGFP); Tg(ins:NTR-P2A-mCherry)*. Mean \pm SD;
991 Kruskal-Wallis test; *ns*: not significant, $**P < 0.005$ (See also Figure 6-Source Data 1).

992 B) *In vivo* time lapse of the main islet of a 4 dpf *Tg(sst1.1:eGFP); Tg(ins:NTR-P2A-mCherry)*
993 larva following β -cell ablation from 3 to 4 dpf. 3D representation (B) and one z-plane (B') of
994 the same islet are shown. The arrowheads point at two GFP+ cells (green) that start to express
995 *ins:mCherry* (red) fluorescence between *t0* and *t1* (visible in the same z-plane). The white
996 arrowhead points to a strongly fluorescent *sst1.1:GFP^{high}* cell. Images were acquired every 30
997 min starting from 4 dpf (96 hpf).

998 C) Volcano plot showing the significant DE genes over- or underexpressed in 20 dpt
999 bihormonal cells versus CTL GFP^{high}/*sst1.1* δ -cells (FC>2, Padj<0.05). The full list of
1000 significant DE genes calculated by DESeq is provided in Figure 6-Source Data 2.

1001 D) Expression in normalized counts of the *sst1.1* and *ins* genes in CTL GFP^{high}/*sst1.1* δ -cells
1002 and bihormonal cells (bi). Padj are calculated by DESeq. *ns*: no significant DE between the
1003 two conditions, $***** < 0.000005$.

1004 E) Top significant KEGG pathways identified among the genes upregulated (in orange) and
1005 downregulated (in green) in bihormonal cells compared to CTL GFP^{high}/*sst1.1* δ -cells. The list
1006 of GO terms below FDR 0.25 is given in Figure 6-Source Data 3 and 4.

1007 F) Immunofluorescence of PCNA and mCherry on paraffin sections through the main islet of
1008 *Tg(ins:NTR-P2A-mCherry)* adult zebrafish, CTL and regenerated (20 dpt after NFP-mediated
1009 ablation), showing PCNA+ nuclei in mCherry+ cells in regenerated islets (confocal images,
1010 white arrowheads).

1011 G) Expression of p53 target genes *mdm2* and *ccng1* mRNA (green) revealed by whole mount
1012 *in situ* hybridization on 6 dpf CTL and ablated *Tg(ins:NTR-P2A-mCherry); Tg(sst1.1:GFP)*

1013 larvae (main islet). Ablation was performed at 3 dpf. Immunodetection of GFP (in red) was
1014 revealed following *in situ* hybridization. White arrowheads point to *sst1.1*:GFP⁺ cells
1015 expressing *mdm2* and *ccng1* after ablation.

1016

1017 **Figure 7. Bihormonal cells can also arise in the pancreatic ducts**

1018 A-B) Whole mount immunodetection of GFP that highlights the ducts (green), mCherry (red)
1019 for β -cells and Sst (grey) on the entire pancreas of *Tg(nkx6.1:eGFP); Tg(ins:NTR-P2A-*
1020 *mCherry)* larvae at 17 dpf. A) CTL larvae showing the main islet in the head and a few
1021 monohormonal endocrine cells (mCherry⁺ or Sst⁺) in the ductal GFP⁺ domain in the tail. The
1022 pancreatic tail is delineated by white dashed lines. B) After treatment with NFP from 3 to 4
1023 dpf, regenerating larvae display scattered bihormonal cells (red and grey) in the tail along the
1024 ducts. Stacks represent 3D projections of confocal images of the whole pancreas. B') Close-
1025 ups of two individual bihormonal cells in the tail (z-planes showing one unique optical
1026 section).

1027 C) Quantification of Sst⁺ mCherry⁺ bihormonal cells based on confocal images. Mann-
1028 Whitney test, **** $P < 0.0001$. (See also Figure 7-Source Data 1).

1029

1030 **Figure 8. Protracted bihormonal cells 4 months after β -cell ablation**

1031 A) Whole mount immunodetection of Ucn3 (red), GFP (green), Ins (grey) on the main islet of
1032 *Tg(sst1.1:eGFP); Tg(ins:NTR-P2A-mCherry)* adult fish revealing persistent bihormonal
1033 GFP⁺ Ins⁺ cells still 4 months after ablation. These cells still also express Ucn3 (white
1034 arrowheads).

1035 B-D) Quantification by flow cytometry of islet cell populations in CTL and 4 months after
1036 ablation. B) mCherry+ GFP+ bihormonal cells. C) mCherry+ GFP- monohormonal β -cells.
1037 Means \pm SD; Unpaired t-test with Welch's correction; * $P < 0.05$

1038

1039

1040 **Figure Supplements legends**

1041 **Figure 1-figure supplement 1. Top 25 genes expressed in regenerated β -cells**

1042 mCherry+ cells from the main islet were sorted by FACS from *Tg(ins:NTR-P2A-mCherry)*
1043 adult zebrafish 2 months after β -cell ablation and gene expression levels were determined by
1044 RNA sequencing (expressed as normalized read counts). The *ins* gene is the highest expressed
1045 gene just above *sst1.1*. This is the result of one single exploratory replicate.

1046

1047 **Figure 1-figure supplement 2. *Tg(sst1.1:GFP)* is active in *sst1.1*+ cells and not in β -cells**

1048 A) Whole mount *in situ* hybridization on 3 dpf *Tg(sst1.1:GFP)* embryo using a *sst1.1*
1049 antisense RNA probe (red) combined with immunodetection of the GFP protein (green)
1050 revealing co-localization between endogenous *sst1.1* transcripts and GFP cells.

1051 B) Whole mount immunofluorescence in the main islet of adult non-ablated (CTL)
1052 *Tg(sst1.1:GFP); Tg(ins:NTR-P2A-mCherry)* fish showing co-localization between GFP
1053 (green) and the endogenous SST protein (red) and not with mCherry β -cells (grey).

1054

1055 **Figure 1-figure supplement 3. Analysis of *sst1.1:GFP* and *ins:NTR-P2A-mCherry*** 1056 **fluorescent cells by flow cytometry**

1057 FACS plot showing GFP and mCherry fluorescence analysis by flow cytometry of dissociated
1058 main islets (3-4 pooled islets) isolated from *Tg(sst1.1:GFP);Tg(ins:NTR-P2A-mCherry)*
1059 control (CTL), 3 dpt and 20 dpt adult fish. Representative plots showing fluorescent cells
1060 along GFP and mCherry axes. The populations of interest are delimited with dashed lines.

1061

1062 **Figure 2-figure supplement 1. Bihormonal cell formation following β -cell ablation with**
1063 **Diphtheria Toxin A**

1064 β -cell ablation performed using the cytotoxic Diphtheria Toxin chain A (DTA) inducible
1065 system in *Tg(ins:loxP-mCherry-loxP-DTA); Tg(ins:CRE-ERT2)*. 7 dpf larvae were treated
1066 with 4-OHT to trigger the recombination of the loxP-mCherry-loxP cassette and allow DTA
1067 expression and β -cells death, and then analysed 9 days after by immunofluorescence. Like in
1068 the NTR/prodrug system, DTA induces the formation of Ins⁺ Sst⁺ bihormonal cells.

1069

1070 **Figure 3-figure supplement 1. Gcg is not detected in bihormonal cells**

1071 Whole mount immunodetection of GFP (green), mCherry (red) and GCG (grey) adult
1072 *Tg(sst1.1:GFP); Tg(ins:NTR-P2A-mCherry)* main islets in CTL and 20 dpt conditions
1073 showing bihormonal (GFP⁺ mCherry⁺) cells at 20 dpt and non-overlapping GCG staining
1074 (white arrowheads).

1075

1076 **Figure 3-figure supplement 2. Table of the main transcription factors considered in this**
1077 **study, their expression and comparison between zebrafish and mouse/human.**

1078

1079 **Figure 5-figure supplement 1. *sst1.1*:GFP expression delineates two distinct δ -cell**
1080 **subpopulations**

1081 A) Fluorescence analysis by flow cytometry of GFP⁺ mCherry⁻ cells from *Tg(sst1.1:eGFP)*;
1082 *Tg(ins:NTR-P2A-mCherry)* islets. Two populations, namely GFP^{high} and GFP^{low}, can be
1083 identified based on their GFP intensity.

1084 B) Heatmap representation of the transcriptomes of GFP^{high} and GFP^{low} cells (3 replicates
1085 each) (significant DE genes).

1086 C) Whole mount *in situ* hybridization on 3 dpf *Tg(sst1.1:GFP)* embryo using a *sst2* antisense
1087 RNA probe (red) combined with immunodetection of the GFP protein (green) revealing co-
1088 localization between endogenous *sst2* transcripts (red) and GFP^{low} + (green) cells (red
1089 arrows). In contrast, GFP^{high} cells do not present detectable transcripts of *sst2*.

1090

1091 **Figure 6-figure supplement 1. Analysis of proliferation in the main islet of adults and**
1092 **larvae during regeneration**

1093 A) Immunofluorescence of PCNA and Pdx1 on paraffin sections through the main islet of
1094 *Tg(ins:NTR-P2A-mCherry)* adult zebrafish in CTL, 3 dpt and 20 dpt conditions. Double
1095 positive PCNA⁺ Pdx1⁺ cells are indicated by white arrows (confocal images). Pdx1⁺ cells
1096 comprise β , *sst1.1* δ and bihormonal cells.

1097 Left graph: Quantification of Pdx1⁺ cells per islet surface measured on several sections from
1098 4-5 different islets. Note the decrease of the density of Pdx1⁺ nuclei at 3 and 20 dpt consistent
1099 with the loss of β -cells. **** <0.0001 ; Mean \pm SD; One-way ANOVA Kruskal-Wallis test
1100 with Dunn's multiple comparisons test.

1101 Right graph: Percentage of Pdx1+ PCNA+ cells versus the total number of Pdx1 cells. CTL,
1102 $0.9 \pm 0.7 \%$; 3 dpt: $18.5 \pm 6.8 \%$; 20 dpt, $16.6 \pm 9.5\%$. $P^{***} < 0.001$, $**** < 0.0001$; Mean \pm
1103 SD; One-way ANOVA Kruskal-Wallis test with Dunn's multiple comparisons test.

1104 B) EdU incorporation in *Tg(ins:NTR-P2A-mCherry); Tg(sst1.1:GFP)* larvae. After ablation
1105 from 3 to 4 dpf, EdU was administered from 4 until 6 dpf (3 dpt). Monohormonal GFP+ cells
1106 and mCherry+ β -cells show basal EdU incorporation at this stage (CTL). After ablation
1107 (NFP), most monohormonal mCherry+ β -cells are EdU negative compared to CTL, leading to
1108 a reduced ratio of EdU+ mCherry+ cells versus total mCherry+ cells (20% in CTL to 7% in
1109 NFP). Like in adults, monohormonal GFP+ cells decreased in NFP-treated samples. They
1110 show variable EdU positivity among larvae (1 to 6 cells in CTL and 0 to 5 cells in NFP) and
1111 the average ratio of EdU+ GFP+ versus total GFP+ cells at CTL (16%) and NFP (23%) is not
1112 significantly different. Bihormonal cells are detected in the NFP condition (8.23 ± 1.8 cells)
1113 and the number of EdU+ bihormonal cells ranges from 0 to 4 cells between larvae with an
1114 average proportion of 19%. Mean \pm SD; *ns*: not significant; $P^{**} < 0.01$, $*** < 0.001$; Mann-
1115 Whitney tests.

1116

1117 **Figure 6-figure supplement 2. Effect on bihormonal cells of different candidate signals**
1118 **linked to the destruction of β -cells.**

1119 A) Bihormonal cell quantification in *Tg(ins:NTR-P2A-mCherry); Tg(sst1.1:GFP)* larvae
1120 exposed for 3 days to 3% D-glucose or mannitol as control, to 10 mM H₂O₂, or to a
1121 combination. mCherry+ GFP+ were quantified.

1122 B) β -cell ablation was performed in *Tg(ins:NTR-P2A-mCherry); Tg(sst1.1:GFP)* larvae from
1123 3 to 4 dpf then the Insulin/PI3K signalling was inhibited by treatment with the PI3K inhibitor

1124 LY294002 from 4 to 6 dpf. mCherry+ GFP+ were quantified. Mean \pm SD; *ns*: not significant,
1125 *P*****<0.0001. Two-way ANOVA test with Tukey's multiple comparison test.

1126

1127 **Figure 7-figure supplement 1. Time course of normal β and sst1.1 δ -cells differentiation**
1128 **from intrapancreatic ducts in the tail of *Tg(nkx6.1:eGFP; Tg(ins:NTR-P2A-mCherry)***
1129 **control larvae.**

1130 Illustrative whole mount immunodetection on the whole pancreas of non-ablated (CTL)
1131 *Tg(nkx6.1:eGFP; Tg(ins:NTR-P2A-mCherry)* larvae labelled with GFP to identify the
1132 pancreatic ductal domain (dotted lines), mCherry (red) and Sst (grey). Monohormonal
1133 mCherry+ and Sst+ cells in the ducts were quantified from 7 to 17 dpf based on the confocal
1134 images.

1135

1136 **List of Figure-Source Data**

1137 Figure 1-Source Data 1

1138 Figure 1-Source Data 2

1139 Figure 3-Source Data 1

1140 Figure 3-Source Data 2

1141 Figure 3-Source Data 3

1142 Figure 3-Source Data 4

1143 Figure 4-Source Data 1

1144 Figure 4-Source Data 2

- 1145 Figure 5-Source Data 1
- 1146 Figure 5-Source Data 2
- 1147 Figure 5-Source Data 3
- 1148 Figure 5-Source Data 4
- 1149 Figure 5-Source Data 5
- 1150 Figure 6-Source Data 1
- 1151 Figure 6-Source Data 2
- 1152 Figure 6-Source Data 3
- 1153 Figure 6-Source Data 4
- 1154 Figure 7-Source Data 1

Figure 1 with 3 supplements and 2 Source Data

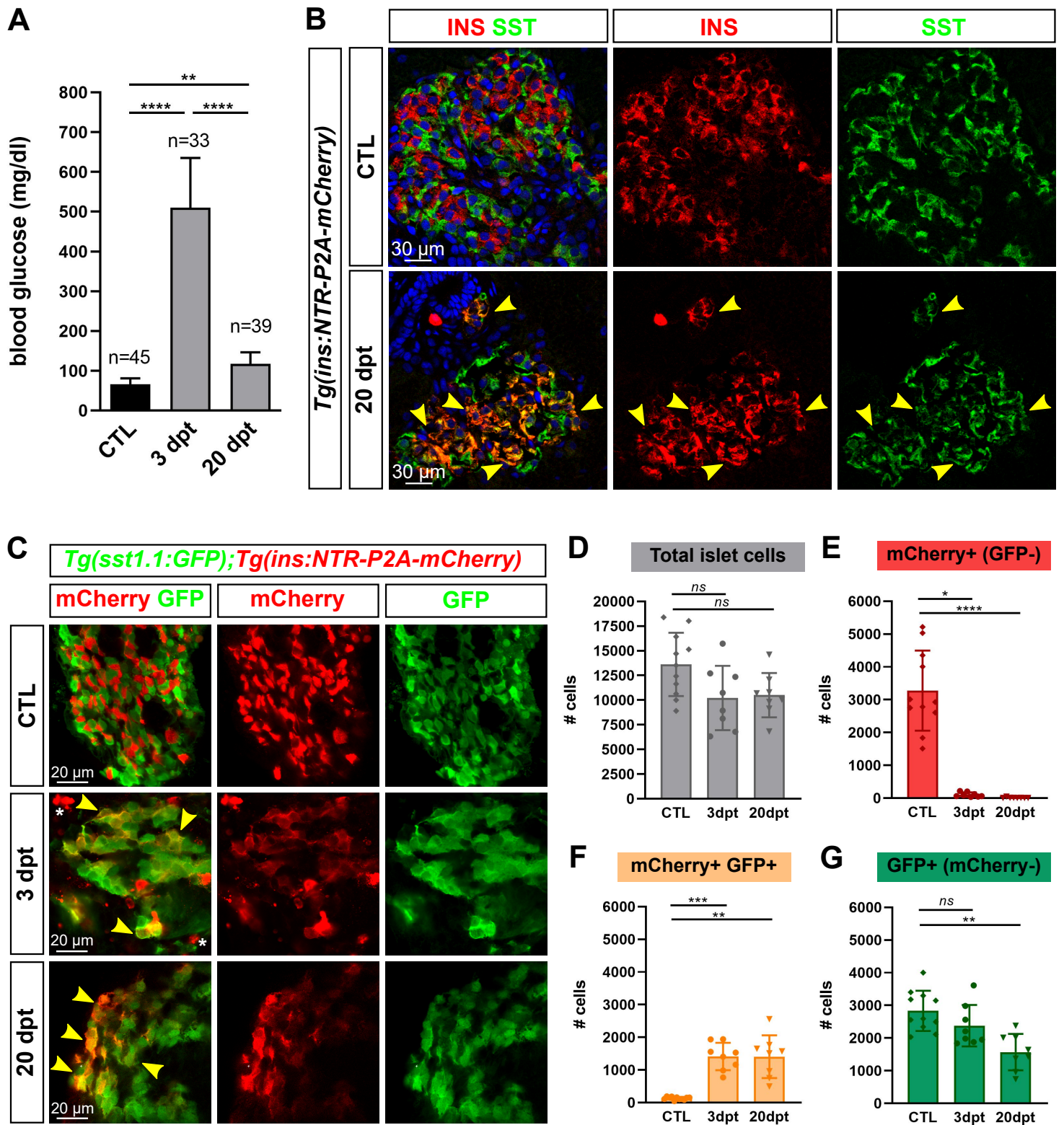


Figure 2 with 1 supplement

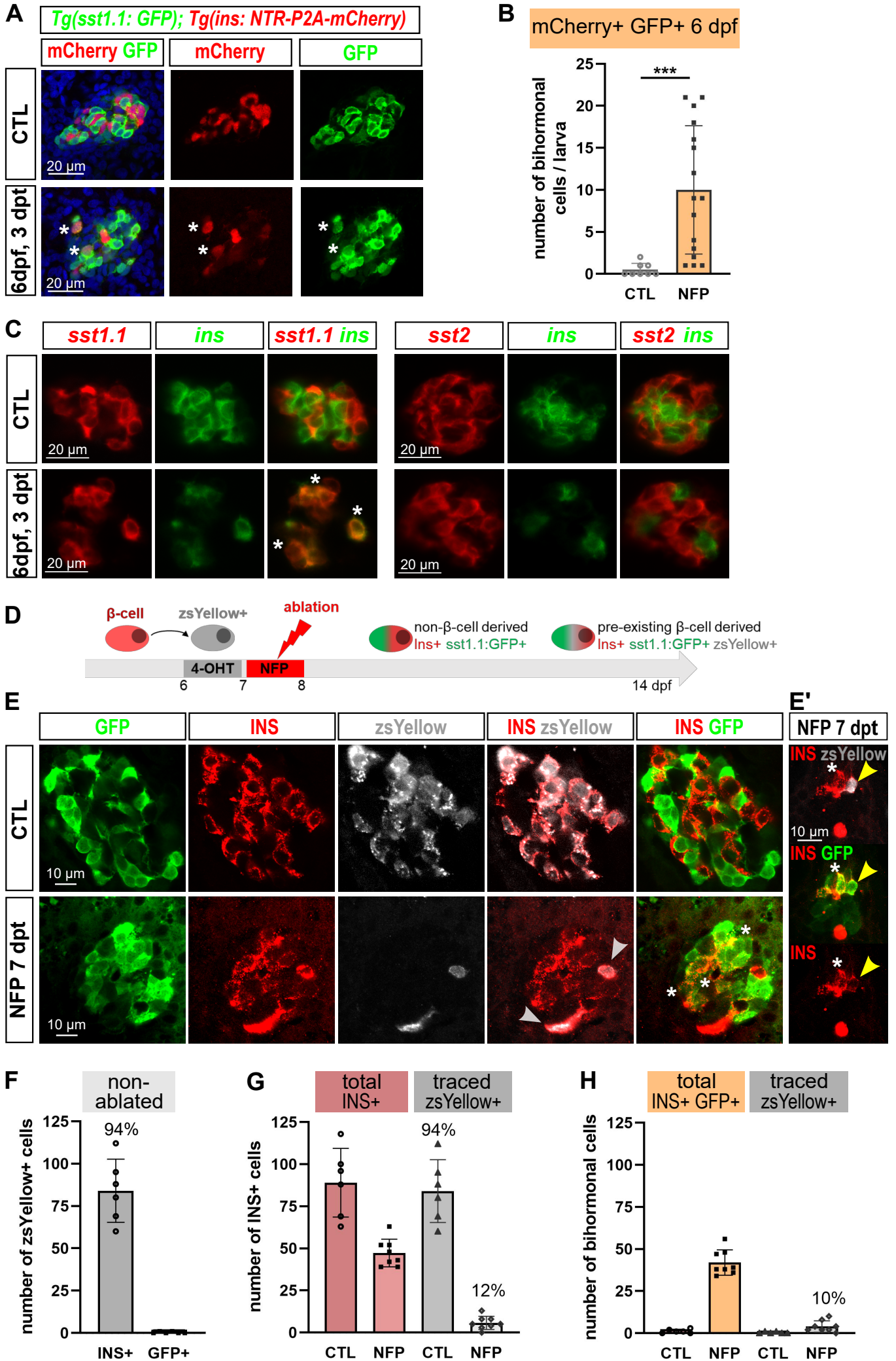


Figure 3 with 2 supplements and 4 Source Data

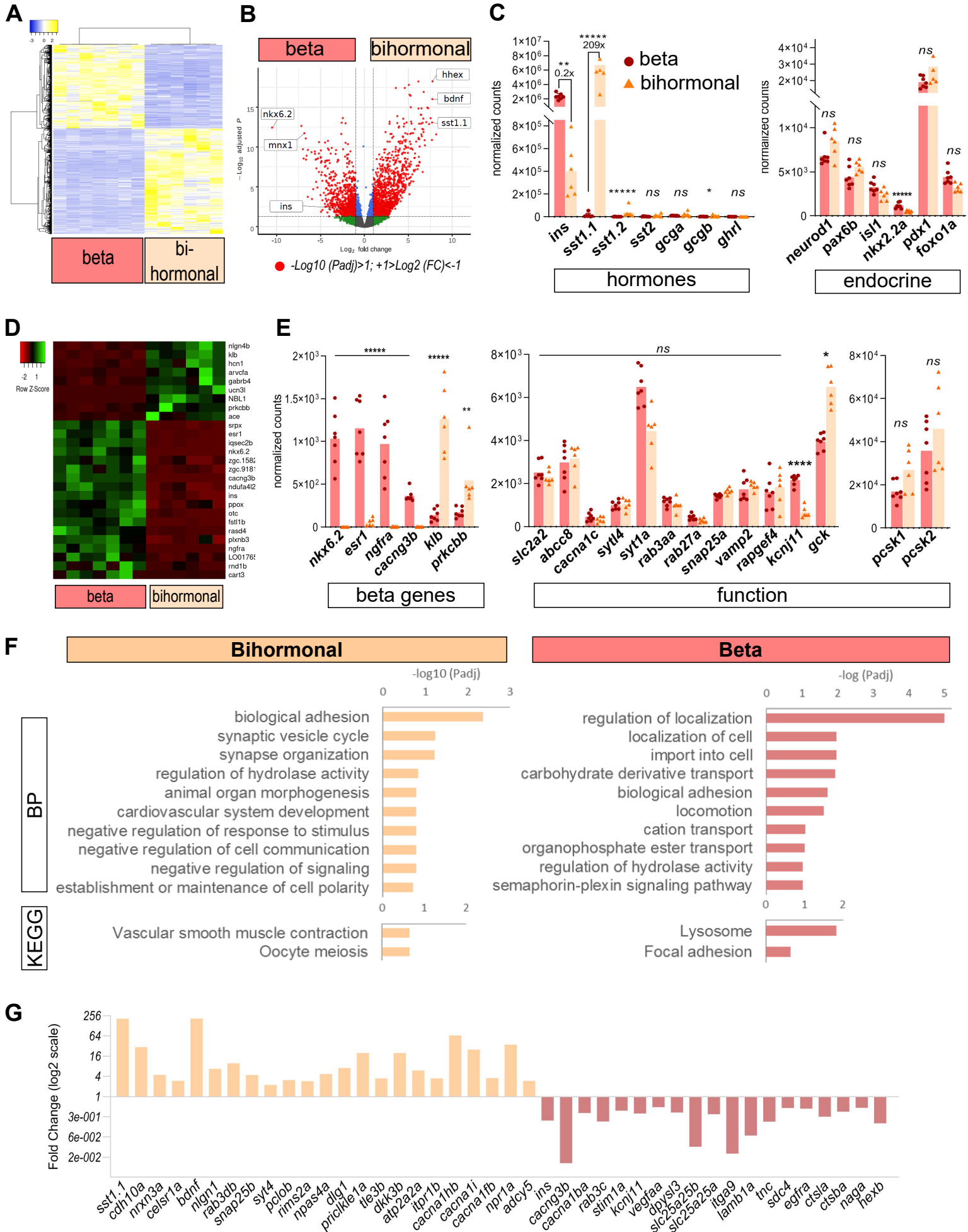


Figure 4 with 2 Source Data

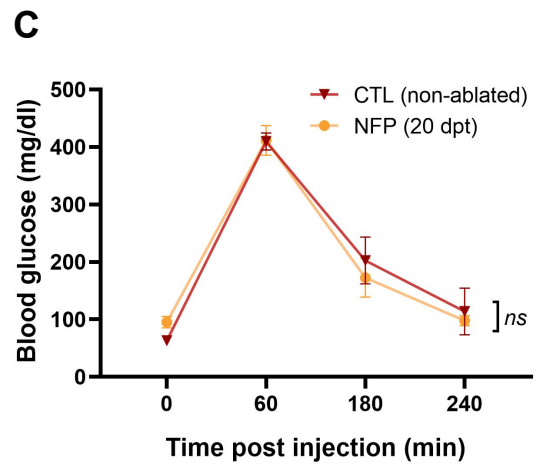
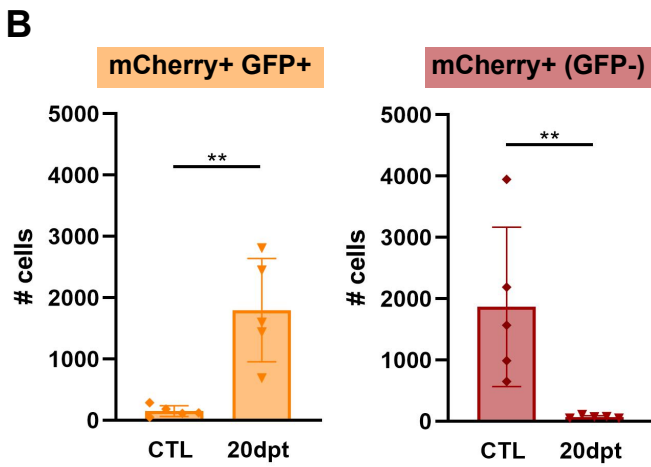
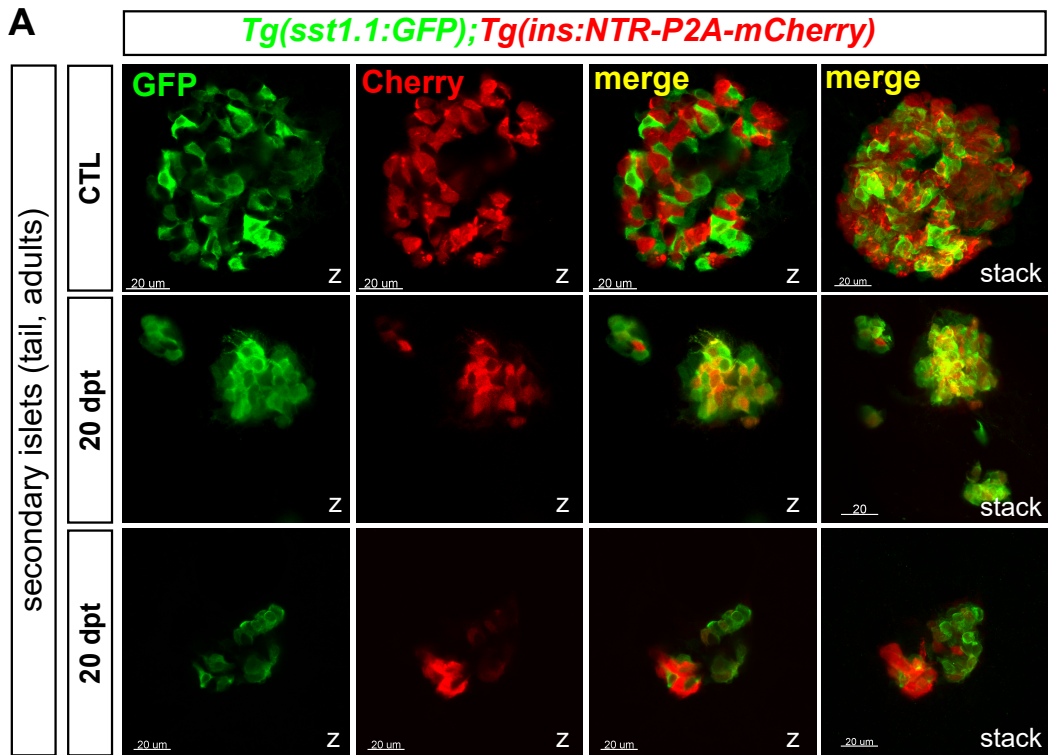


Figure 5 with 1 supplement and 5 Source Data

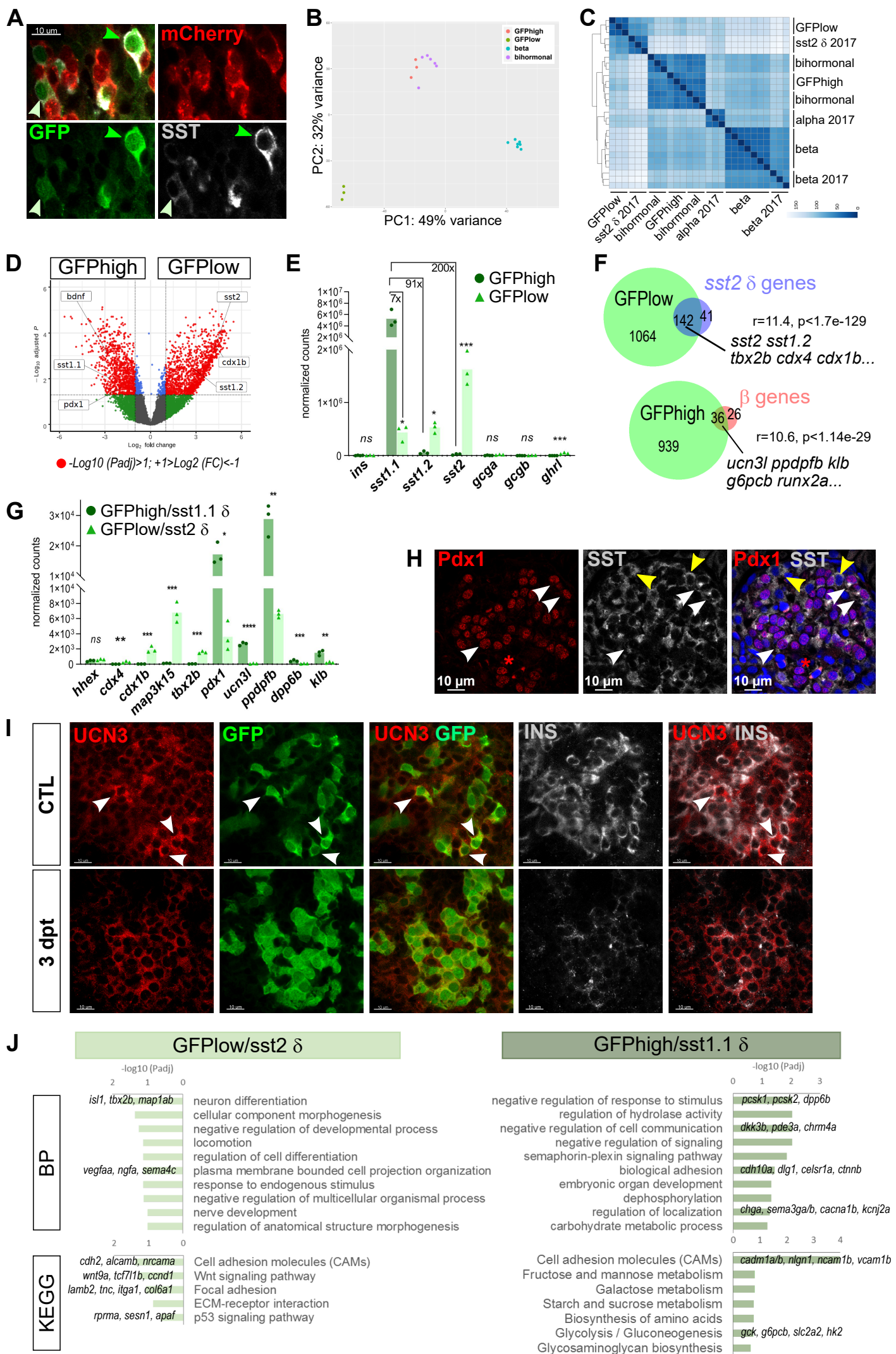


Figure 6 with 2 supplements and 4 Source Data

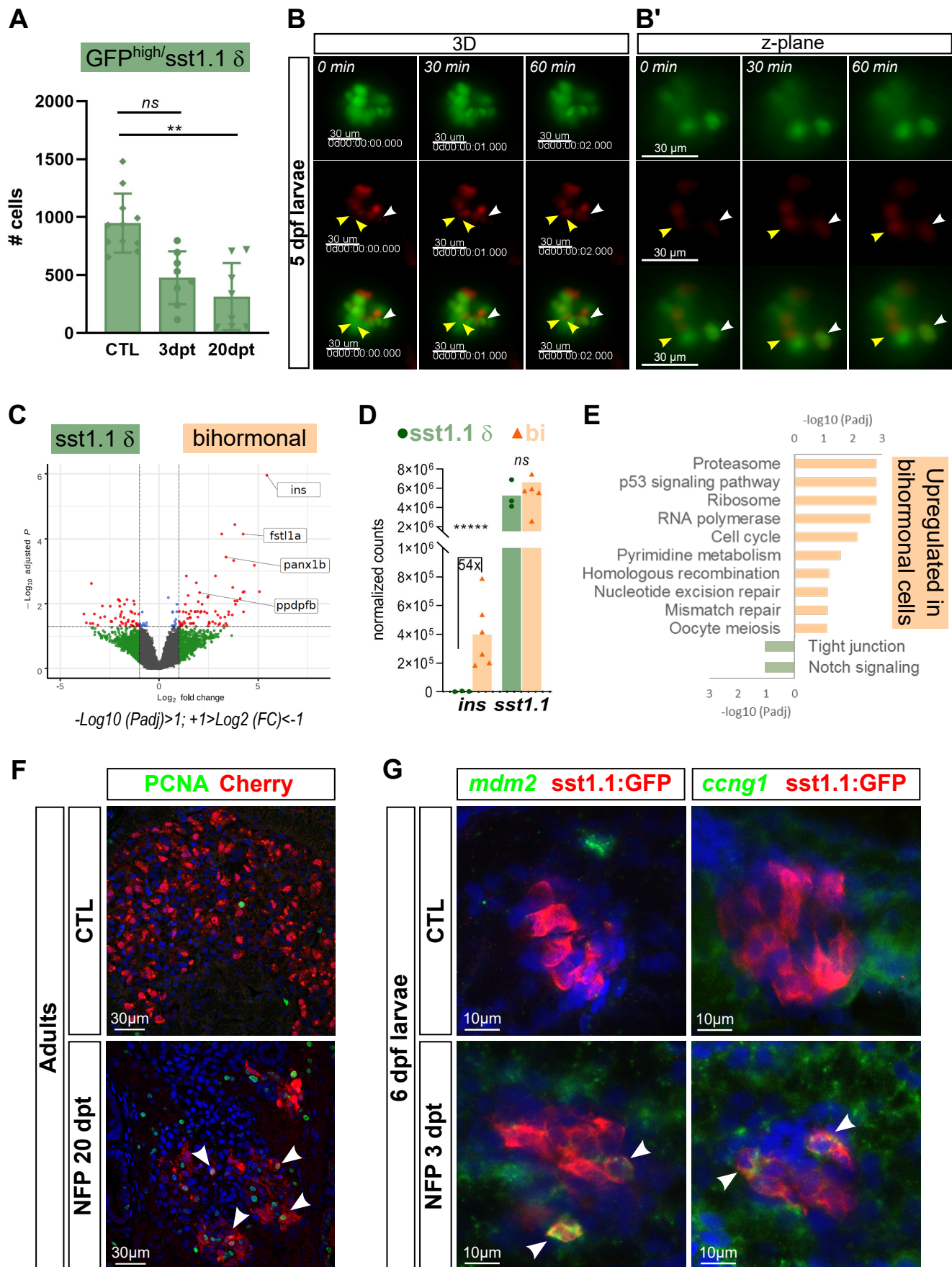
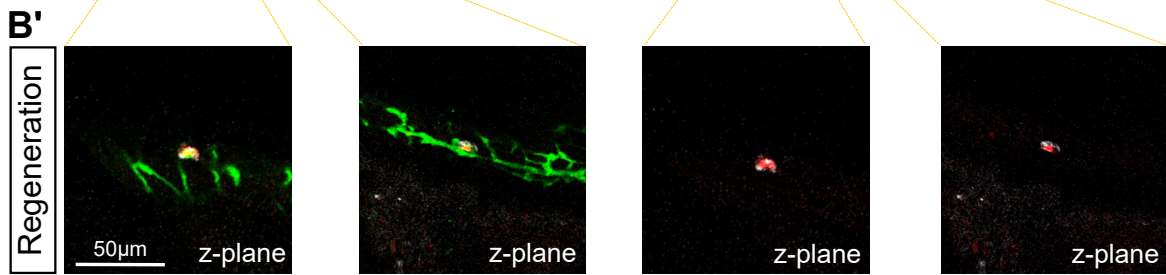
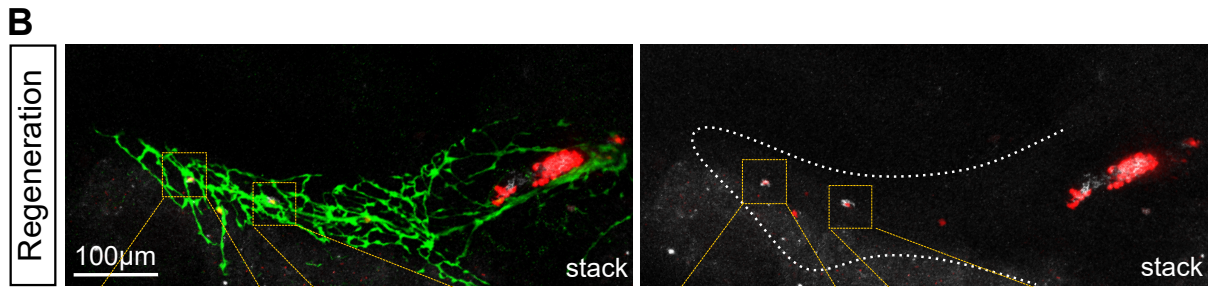
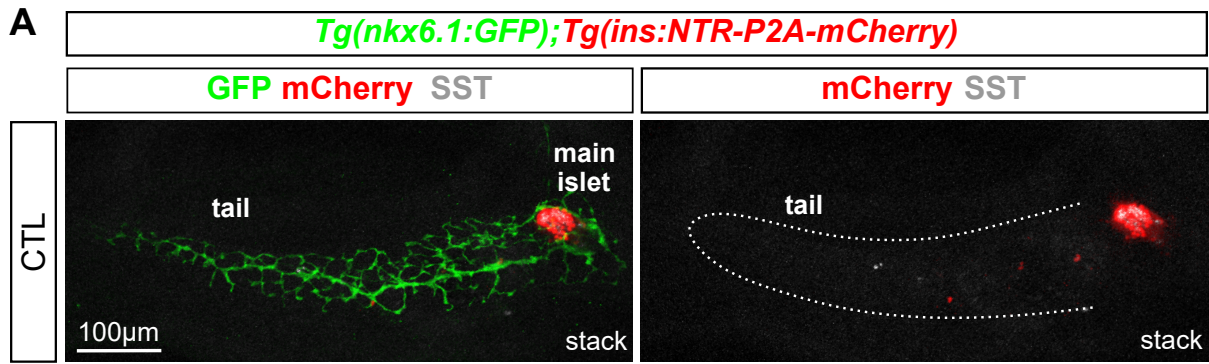


Figure 7 with 1 supplement and 1 Source Data



C

Sst+ Cherry+ in the ducts

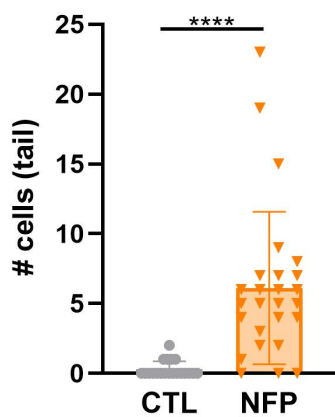
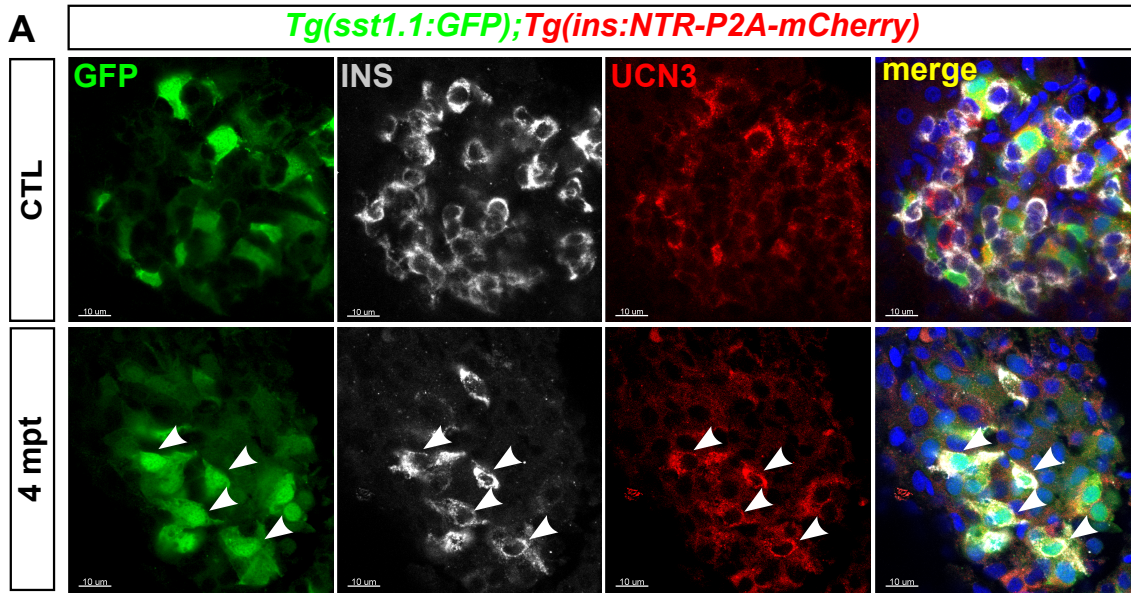
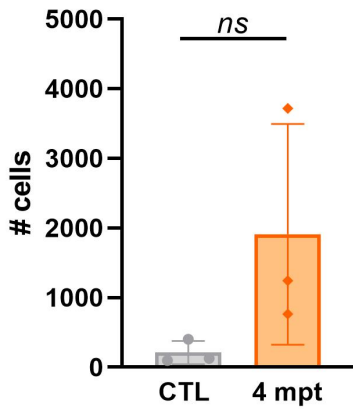


Figure 8



B Bihormonal



C mCherry+ GFP-

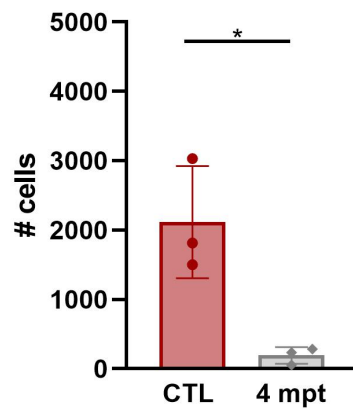
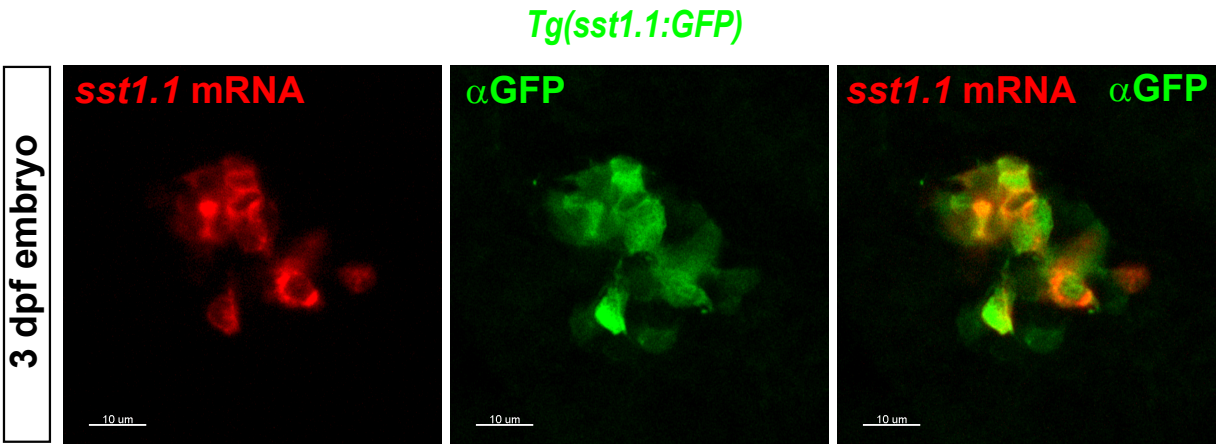


Figure 1-figure supplement 1

Gene_Name	Expression in regenerated β-cells
ins	14801223
sst1.1	7912534
mt-co1	435554
ppdpfb	267739
rgs5a	256637
dkk3b	213588
mt-co2	210445
RPL41	206138
scg3	146678
calca	143619
pcsk1	137921
eef1a1l2	133915
fosab	130543
tmsb1	130150
cst3	125586
mt-co3	107003
rpl19	95153
pcsk2	94936
rpsa	91191
mt-cyb	89586

Figure 1-figure supplement 2

A



B

Tg(sst1.1:GFP);Tg(ins:NTR-P2A-mCherry)

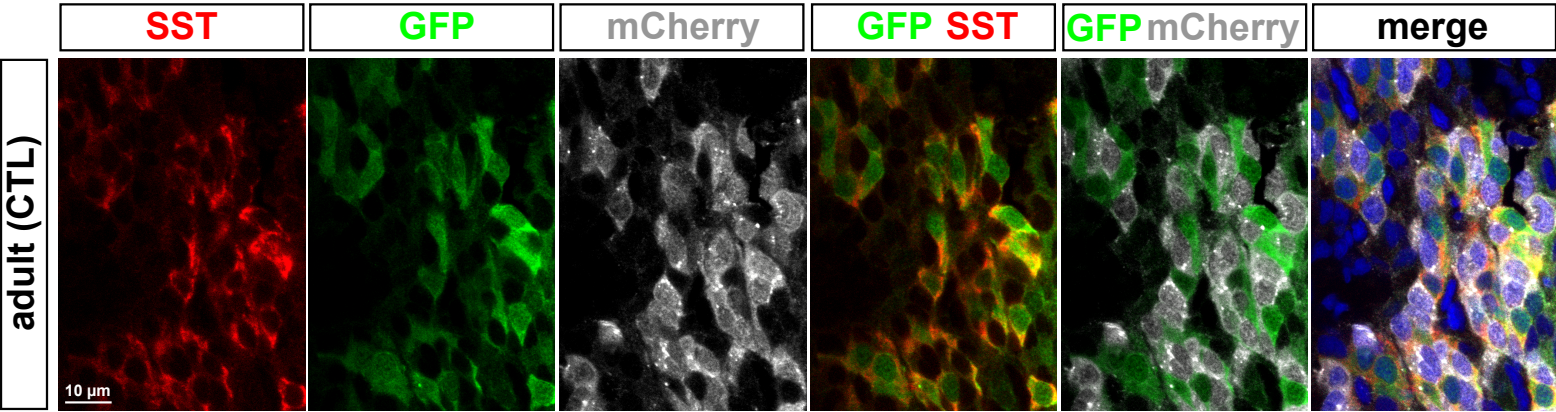


Figure 1-figure supplement 3

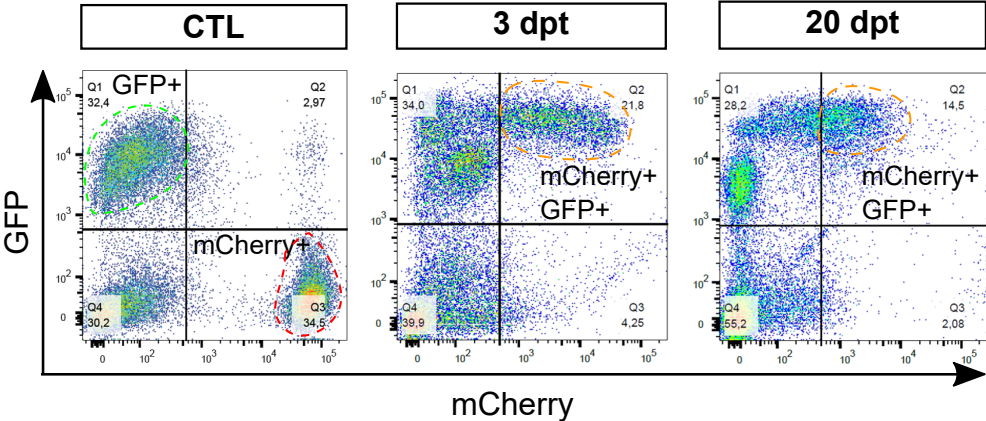
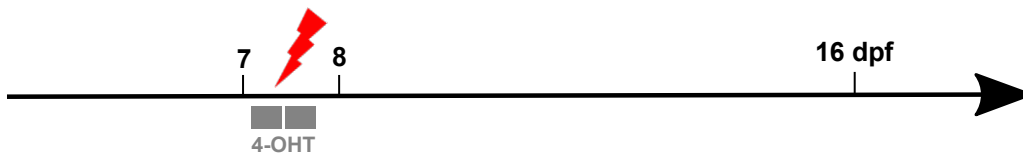


Figure 2-figure supplement 1

DTA-mediated β -cell ablation triggered by 4-OHT



Tg(ins:loxP-mCherry-loxP-DTA); Tg(ins:CRE-ERT2)

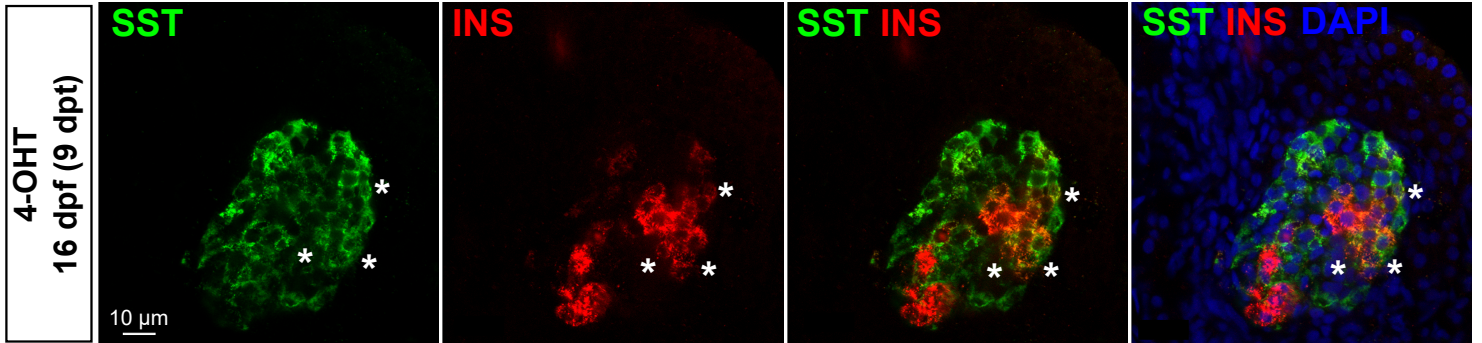


Figure 3-figure supplement 1

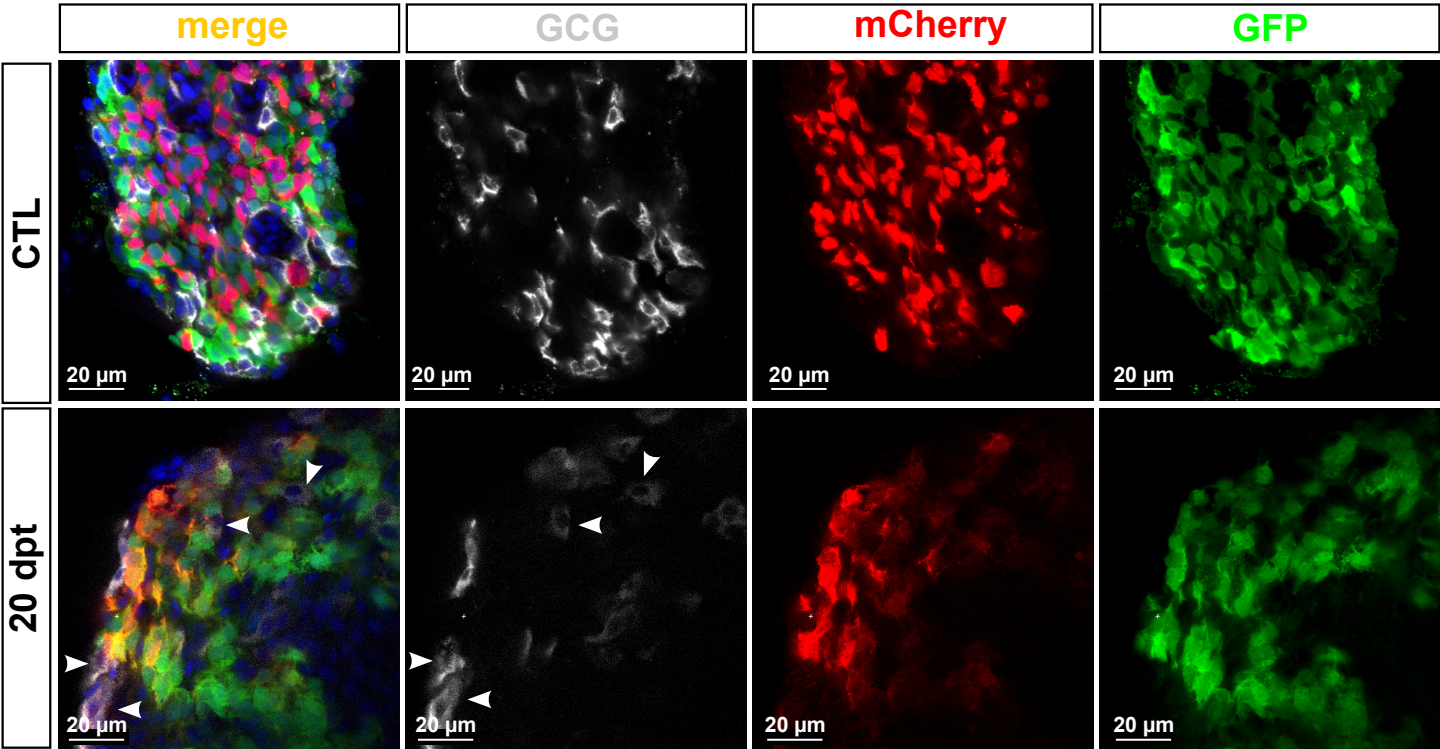


Figure 3-figure supplement 2

Transcription factor	Expression in mouse/human islets (mature/adults)	Zebrafish orthologue	Expression in zebrafish islets (mature/adults)	Functional orthologue/paralogue or equivalent in zebrafish
<i>Neurod1</i>	Pan-endocrine	<i>neurod1</i>	Pan-endocrine	
<i>Pax6</i>	Pan-endocrine	<i>pax6b</i>	Pan-endocrine	<i>pax6b</i>
<i>Isl1</i>	Pan-endocrine	<i>isl1</i>	Pan-endocrine	
<i>Pdx1</i>	β -cells, δ -cells	<i>pdx1</i>	β -cells, sst1.1 δ -cell (this study)	
<i>Nkx6.1</i>	β -cells	<i>nkx6.1</i>	Not expressed in mature islet cells	<i>nkx6.2</i> in β -cells
<i>Nkx6.2</i>	Not detected in mature islet cells	<i>nkx6.2</i>	β -cells	
<i>Mnx1</i>	β -cells	<i>mnx1</i>	β -cells and α -cells	
<i>Hhex</i>	δ -cells	<i>hhex</i>	δ -cells	

Transcription factor	Expression in mouse/human pancreatic progenitors	Zebrafish orthologue	Expression in pancreatic progenitors	Functional orthologue/paralogue or equivalent in zebrafish
<i>Ascl1</i> (previously <i>Mash1</i>)	Not expressed in mature islet cells	<i>ascl1b</i>	Not expressed in mature islet cells	<i>ascl1b</i>
<i>Neurog3</i>	Endocrine progenitors. Not expressed in mature islet cells	<i>neurog3</i>	No expression in zebrafish pancreas	<i>ascl1b</i> and <i>neurod1</i> in embryonic progenitors
<i>Nkx6.1</i>	Pancreatic embryonic progenitors (ducts)	<i>nkx6.1</i>	Pancreatic embryonic progenitors and duct cells	
<i>Sox9</i>	Pancreatic embryonic progenitors	<i>sox9b</i>	Pancreatic embryonic progenitors	<i>sox9b</i>
<i>Pdx1</i>	Pancreatic embryonic progenitors and duct cells	<i>Pdx1</i>	Pancreatic embryonic progenitors and duct cells	

Figure 5-figure supplement 1

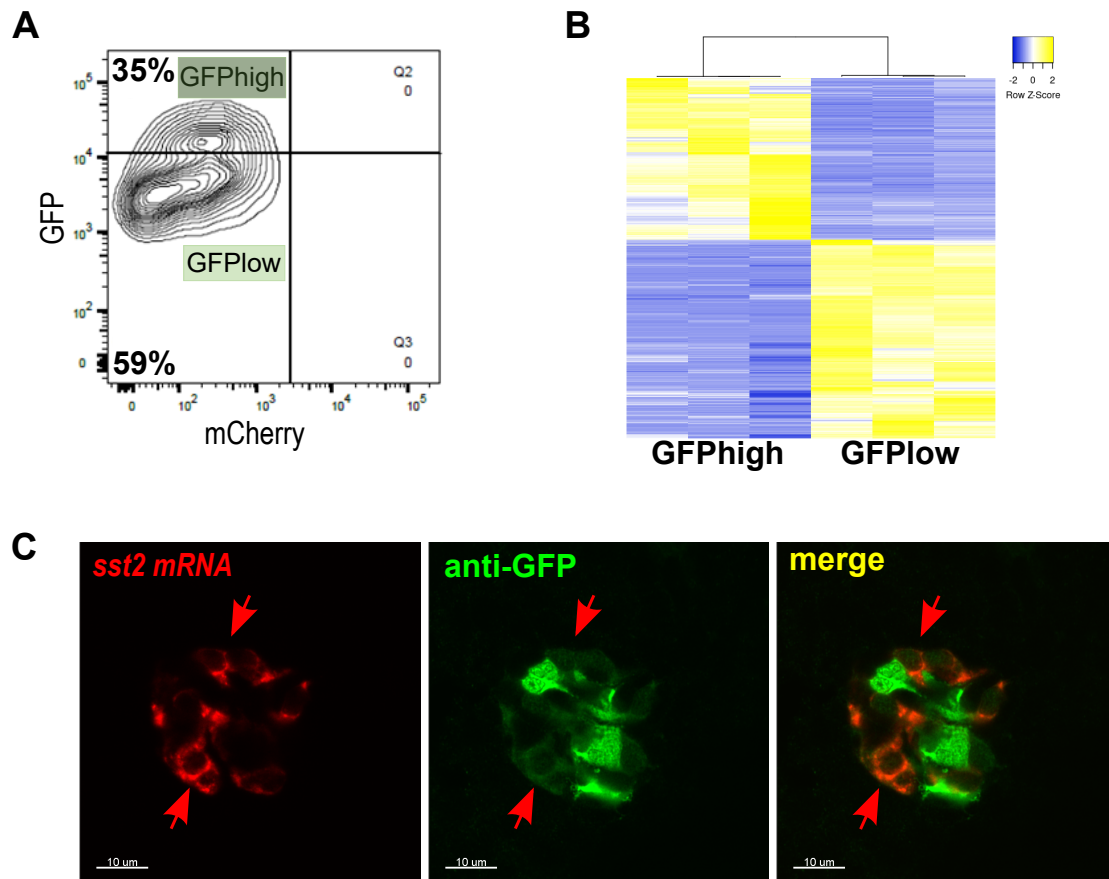


Figure 6-figure supplement 1

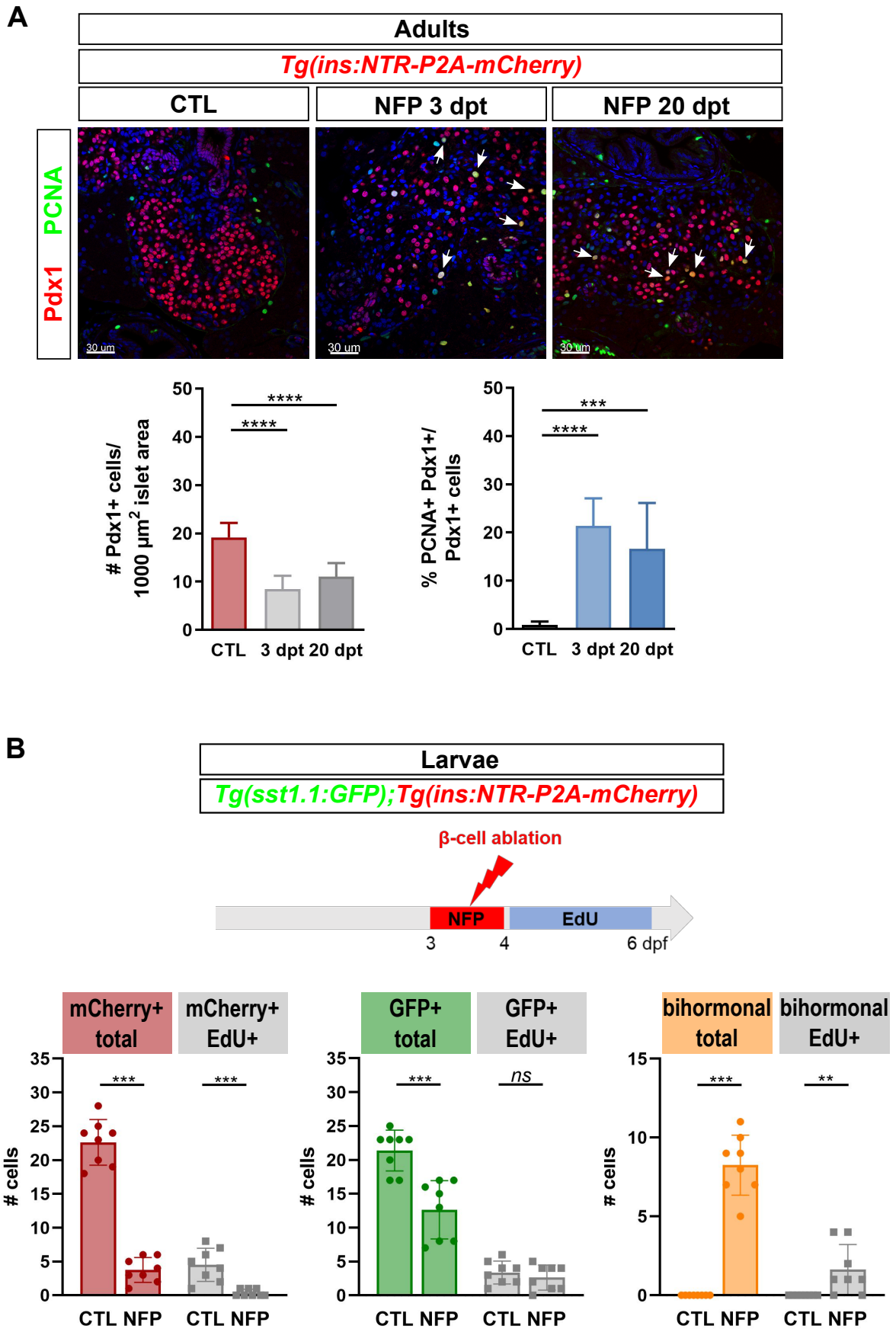


Figure 6-figure supplement 2

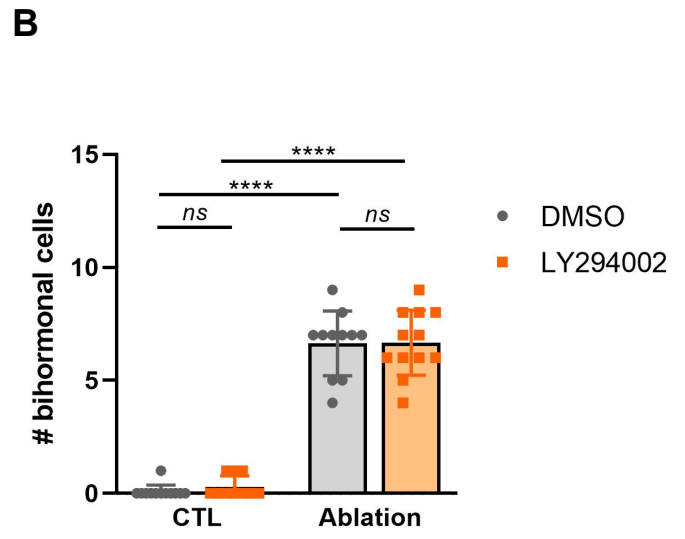
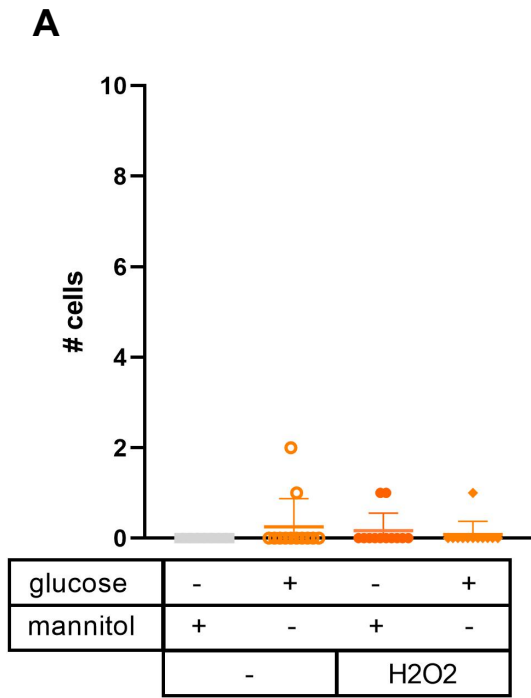


Figure 7-figure supplement 1

